Preprints (www.preprints.org) | NOT PEER-REVIEWED | Posted: 21 October 2021 doi:10.20944/preprints202110.0308.v1

Article

Ɛ34 Phage Tailspike Protein is Resistant to Trypsin and Inhibits and Salmonella Biofilm Formation

Joseph A. Ayariga[1]*, Logan Gildea[2], Robert Villafane[3]

[1] The Biomedical Engineering Program, College of Science, Technology, Engineering and Mathematics (C-STEM), Alabama State University, 1627 Hall Street, Montgomery, AL, 36104; jayariga7546@myasu.alasu.edu/ayarigajosephatia@yahoo.co.uk

[2] The Microbiology Program, College of Science, Technology, Engineering and Mathematics (C-STEM), Alabama State University, Montgomery, AL, 36104

[3] Department of Biological Sciences, Microbiology PhD. Program, College of Science, Technology, Engineering and Mathematics (C-STEM), Alabama State University, 1627 Hall Street Montgomery, Alabama 36104

* Correspondence: jayari-ga7546@myasu.alasu.edu/ayarigajosephatia@yahoo.co.uk

Abstract: *Salmonella* can cause acute and chronic infections in humans. *Salmonella* species are known to cause food poisoning and other diseases in developing countries. Their role in the pathogenesis of these diseases has received increased international attention. Despite numerous advances in sanitation, they still can infect humans and cause outbreaks in developed countries. For example, *Salmonella* causes about 1.2 million illnesses in the US each year with over 450 deaths. Additionally, *Salmonella* outbreaks cause significant losses to chicken producers globally. The *Salmonella* species is also prone to acquiring resistance to various classes of antibiotics. Hence, the need for a paradigm shift from antibiotics to bacteriophages to manage, control and treat bacterial infections. The ε34 phage belongs to Podoviruses and categorized into the P22-like phages. The P22-like phages include ε34, ES18, P22, ST104, and ST64T. In this work, we investigated the antibacterial property of ε34 phage tailspike protein against *Salmonella newington* (*S. newington*). We demonstrate here that, the phage's tailspike protein enzymatic property as a LPS hydrolase synergizes with Vero Cell culture supernatant in killing *S. newington*. Using decellularized cartilage scaffold as an ex vivo tissue model, the ε34 TSP protected the scaffold from *S. newington* biofilm formation. Computational analysis of the ε34 TSP interaction with membrane proteins of *S. newington* demonstrated a higher probability (0.7318) of binding to ompA of *S. newington*, and when docked to ompA extracellular component, it produced a high free energy of -11.3kcal/mol. We also demonstrate the resistance/sensitivity of the tailspike to the digestive enzyme trypsin. The data obtained in this work indicates that the trypsin resistant tailspike protein of Ɛ34 phage can be formulated as a novel antibacterial agent against *S. newington*.

Keywords: *Salmonella newington*; ε34 phage; Lipopolysaccharides; Antibacterial

1. Introduction

Resistance to antibiotics is common among pathogenic bacteria **[1-4].** In a study, Lopatkin et al. discovered that mutations in key metabolic genes can affect microbial metabolism and evolve resistance **[5]**. Antibiotic resistance explains why most treatments fails with antibiotics **[6-8]**, and most bacterial resistance are often initiated by acquiring a genetic mutation that limits the ability of an antibiotic to attack its target **[9,10]**. This resistance can also be triggered by various cellular factors, such as the presence of a certain type of gene or the transfer of another gene **[11]**. More so, antibiotic resistance mutation can appear in many ways, for instance, it can modify an antibiotic's ability to interact with a particular cell or its promoter regions **[12]**. For example, the antibiotic resistance alleles, such as genes encoding β-lactamases, commonly appear in mobile genetic elements and can become exchanged by horizontal gene transfer **[13,14].**

Salmonella can cause acute and chronic infections in humans. Their role in the pathogenesis of these diseases has received increased international attention. Salmonella causes about 1.2 million illnesses in the US each year.

© 2021 by the author(s). Distributed under a Creative Commons CC BY license.

Preprints (www.preprints.org) | NOT PEER-REVIEWED | Posted: 21 October 2021 doi:10.20944/preprints202110.0308.v1

Around 450 individuals die due to this illness. It is considered a life-threatening illness **[15].** Additionally, Salmonella outbreaks cause significant losses for chicken producers globally **[16]**. Salmonella species are known to cause food poisoning and other diseases in developing countries. Despite numerous advances in sanitation, they still can infect humans and cause outbreaks in developed countries. The Salmonella species is also prone to acquiring resistance to various classes of antibiotics. Hence, the new paradigm is the shift from antibiotics to bacteriophages to manage, control and treat bacterial infections. The potential of bacterial viruses as antibacterial agents was widely recognized during the first century **[17]**. Their use as therapeutics has declined due to the emergence and success of antibiotics, however, in current times, there is renewed interest in phages as a biocontrol strategy and their molecular components offers a broad perspective on how to combat bacterial infections **[18].**

Several bacteriophages specific to Salmonella have been isolated and categorized into five groupings (P27-like, P2-like, lambdoid, P22-like, and T7-like) and three outliers (ε15, KS7, and Felix O1). While the P27 group includes ST64B; Fels-2, SopEφ, and PSP3 represents the P2 group; the lambdoid Salmonella phages include Gifsy-1, Gifsy-2, and Fels-1. The P22-like phages include ε34, ES18, P22, ST104, and ST64T. SP6 forms the lone member of the T7-like group **[19].** Ɛ34 phage belongs to the P22-like phages **[20-22].** The tailspike protein of Ɛ34 phage possesses similar functionality and structural stability as the P22 phage tailspike protein, and it is the functional component used in the phage's adsorption to its host **[23]**. The unique predicted structure of this protein consists of a globular head binding domain, a solenoid-shape parallel beta-helix domain required in LPS binding, and a beta-prism domain uncharacteristically identical to the well-known P22 tailspike protein.

In cell culture, cells produce several antimicrobial agents that are release into the media as defense tactic against pathogens. For instance, cell-mediated immunity against bacteria involves the production of cytokine, chemokines, pro-inflammatory cytokines, anti-inflammatory cytokines etc. **[24].** A special example is the expression of interleukin-12, a crucial signal of the innate immune system, when toll-like receptors (TLRs) of macrophages are stimulated by bacterial lipoproteins **[25].** Another set of important antimicrobial agents released into cell culture media are nitric oxide and host defense proteins. Nitric oxide has been demonstrated to possess strong bactericidal property **[26],** whereas host defense proteins are natural molecules that fight against pathogens. Host defense proteins have been demonstrated to be found in all living organisms to possess some varying degree of antimicrobial properties **[27,28].** These naturally occurring peptides consist of amino acids that can vary in size from 12 to 50, mainly cationic due to the presence of arginine and excess lysine **[29]**. Host defense Peptides are cationic and can interact with the net negative charged bacteria membranes and penetrate the membranes **[30,31].** Their direct antimicrobial actions against bacteria often involve multiple targets, for instance, they can affect bacterial membrane integrity, block the activity of enzymes and chaperones, inhibit cell wall peptidoglycan biosynthesis, block cell division, inhibit cytosolic RNA, protein, or DNA synthesis, etc**. [32,33].** For example, human μ-defensin-3, hBD-3, has a potent antimicrobial activity against multi-drug resistant *S. aureus* and vancomycin-resistant *Enterococcus faecium* via cell wall perforation **[34].**

Phages or phage derived components can complement host cell defense against bacteria **[35].** Using computational analysis, Roach et al., 2017 demonstrated that successful phage therapy requires at least 20% immune responses in a healthy individual to eliminate phage-sensitive bacterial population in the lungs, whereas 50% was required to eradicate phage resistance ones **[36]**.

In this work, we investigated the antibacterial property of ε34 phage tailspike against *S. newington*. We demonstrate here that, the phage's tailspike enzymatic property as LPS hydrolase synergizes with Vero Cell culture supernatant in killing *S. newington*. Using computational analysis, we showed that the tailspike protein of Ɛ34 phage strongly binds to the outer membrane protein A (ompA) of *S. newington*, thus mediating the bacterial cell lysis via membrane function/integrity disruption. Testing the ability of the tailspike protein to prevent the formation of biofilm on an animal tissue by *S. newington*, we employed decellularized cartilage tissue as an ex vivo model. Pre-treating this scaffold with the tailspike protein prevented biofilm formation on the scaffold. We also demonstrate the resistance of the tailspike to trypsin. Thus, the data obtained in this work indicates that the trypsin resistant tailspike protein of Ɛ34 phage that also shows antimicrobial and antibiofilm formation potency can be an effective and novel therapeutic agent against *S. newington*.

2. Materials and Methods

Preprints (www.preprints.org) | NOT PEER-REVIEWED | Posted: 21 October 2021 doi:10.20944/preprints202110.0308.v1

The cloning, PCR identification, sequence confirmation, protein expression, antibody probing, and the thermal characterization have been documented elsewhere **[37].**

2.1. Ɛ34 Phage antibacterial assay

S. newington cultures in 96 well plates at an OD of 0.2 were infected with Ɛ34 phages at MOIs of 10, 1, 0.1 and 0.01 and the growth kinetics of *S. newington* monitored for 12 h. Growth inhibition kinetics of *S. newington* was assessed by measuring the absorbance at 600 nm with SpectraMax ABS Plus microplate reader (Molecular Devices, Thermo Fisher, USA) at an hourly interval for 12 h at 37 °C. The absorbance values were averaged from 3 replicates and values used to plot graphs. Triplicate experiments were carried out and absorbance reading at 600 nm averaged for each replicate.

2.2. EƐ34 tailspike protein antibacterial assay

S. newington cultures in 96 well plates at an OD of 0.2 were treated to EƐ34 tailspike protein at concentrations of 390 µg/ml EƐ34 TSP, 39 µg/ml EƐ34 TSP, 3.9 µg/ml EƐ34 TSP and 0.39 µg/ml EƐ34 TSP and the growth kinetics of *S. newington* monitored for 12 h. EƐ34 TSP was diluted using 1X PBS. Growth inhibition kinetics of *S. newington* was assessed by measuring the absorbance at 600 nm with SpectraMax ABS Plus Microplate Reader (Molecular Devices, Thermo Fisher, USA) at an hourly interval for 12 h at 37 °C. The absorbance values were averaged from 3 replicates and values used to plot graphs.

2.3. Ɛ34 Phage tailspike protein and Vero cell culture supernatant combination bacteria killing assay

Vero cells were cultured with DMEM media (ATCC, Manassas) containing 10% FBS (ATCC, Manassas) for two days. Afterward, cell culture supernatant was pipetted into a 15 mL tubes and centrifuged at 400 rpm for 5 min and the pellet discarded. The centrifuged supernatant was then aliquot into a fresh sterile 15 mL tube and stored at -20 °C for subsequent use in bacterial study. To investigate the potential of EƐ34 TSP in combination with Vero cell culture supernatant as an efficacious phage therapy combination, we diluted EƐ34 TSP stock sample with Vero cell culture supernatant to achieve a concentrations of 390 µg/ml EƐ34 TSP, 39 µg/ml EƐ34 TSP, 3.9 µg/ml EƐ34 TSP and 0.39 µg/ml EƐ34 TSP in Vero cell culture supernatant. *S. newington* cultures in 96 well plates at an OD of 0.2 were treated with these concentrations and the growth kinetics of *S. newington* monitored for 14 h. Growth inhibition kinetics of *S. newington* was assessed by measuring the absorbance at 600 nm with SpectraMax ABS Plus Microplate Reader (Molecular Devices, Thermo Fisher, USA) at an hourly interval for 12 h at 37 °C. The absorbance values were averaged from 3 replicates and values used to plot graphs.

2.4. Ɛ34 Phage and Vero cell culture supernatant combination bacteria killing assay

To investigate the antibacterial potential of Ɛ34 phage in combination with Vero cell culture supernatant, we diluted Ɛ34 TSP stock sample with Vero cell culture supernatant to achieve phage MOIs of 10, 1, 0.1 and 0.01. *S. newington* cultures in 96 well plates at an OD of 0.2 were infected with these concentrations and the growth kinetics of *S. newington* monitored for 12 h. Experiments were repeated three times and the readings of each replicate averaged. Growth inhibition kinetics of *S. newington* was assessed by measuring the absorbance at 600 nm with SpectraMax ABS Plus Microplate Reader (Molecular Devices, Thermo Fisher, USA) at an hourly interval for 14 h at 37 °C. The absorbance values were averaged from 3 replicates and values used to plot graphs.

2.5. Agar Spot Test for antibacterial properties of EƐ34 TSP or Ɛ34 phage with Vero cell culture supernatant.

The antibacterial activity of EƐ34 TSP or Ɛ34 phage or their combination with Vero cell medias against *S. newington* was tested as previously described **[38,39]** with slight modification. In summary, a 10 µl aliquot from *S. newington* suspension at OD of 0.5 in LB broth was spotted on the surface of LB agar and quickly followed with same volume of EƐ34 TSP or Ɛ34 phage solution or their combination with Vero cell culture supernatant. Agar plates were incubated for 12 and 36 h at 37 °C. The antibacterial activity was determined by the presence or absence of colony forming unit formed after 12 and 36 h time points.

2.6. Enzyme sensitivity test under non-denaturing conditions

1 mg/ml of EƐ34 TSP samples or recombinant enterokinase (rEK) digested samples (also termed matured Ɛ34 TSP (MƐ34 TSP)) of the same protein were initially dialyzed against a buffer consisting of 50 mg/ml tris-HCl, pH 7.4, then mixed with trypsin and incubated at 37 °C in a pre-set water bath, then quenched after 6 h of incubation. Quenching was achieved via the addition of trypsin inhibitor and samples analyzed via 7.5% Native-PAGE and visualized by Coommasie blue staining. Samples were run at 100 volts for 60 min under non-denaturing conditions.

2.7. Enzyme sensitivity test under 2% SDS at physiological temperature

Preprints (www.preprints.org) | NOT PEER-REVIEWED | Posted: 21 October 2021 doi:10.20944/preprints202110.0308.v1

To investigate the structural dynamics of our protein under slightly denaturing conditions, we deployed the use of the denaturing detergent, sodium dodecyl sulfate (SDS) denaturation for 6 h. A sample of 0.5 mg/ml of EƐ34 and MƐ34 TSP were dialyzed against neutral buffer consisting of 50 mg/ml tris-HCl, pH 7.4, this was followed by mixing with 2% SDS then treated with the respective enzyme at 1:20 w/w of enzyme to protein sample. The treated samples were then incubated in a water bath at 37 ˚C for 6 h. Afterward, the proteolytic reactions were stopped by the addition of protease inhibitor at a 10 µg/ml final concentration and the samples electrophoretically analyzed using 10% native polyacrylamide gel. Placebos received buffer instead of the enzyme and heated controls samples also received no treatment at all except heating of these samples in 2% SDS loading buffer at 100 ˚C for 5 min. Samples were run at 100 volts for 250 min under non-denaturing running buffer conditions. Gels were then visualized via Coomassie blue staining, and the gels photographed using ChemiDoc XRS installed with Quantity One.

2.8. Enzyme sensitivity test under increasing concentrations of enzyme

Concentration dependent tryptic proteolysis of EƐ34 TSP at 37 ˚C via a dose dependent treatment of our TSP to trypsin was carried out. In this work; we measured the ability of the enzyme to digest EƐ34 TSP in increasing concentrations of the enzyme (trypsin). 1 mg/ml of EƐ34 TSP samples were initially dialyzed against buffer consisting of 50 mg/ml tris-HCl, pH 7.4 to remove protease inhibitors then mixed with trypsin in differing ratios. A final concentration of 100 µg, 200 µg, 300 µg, 400 µg and 500 µg of trypsin were used to treat 1 mg of EƐ34 TSP. Thus, a protein to enzyme ratio of 100:1, 100:2, 100:3, 100:4, 100:5 respectively for each treatment sample were achieved. Then samples were incubated for 6 h under 37 ˚C. Afterwards samples were run in 7.5% polyacrylamide gel and the gels photographed using ChemiDoc XRS installed with Quantity One. Experiments were repeated thrice and the densitometric values of the resulting gels were recorded via Image J 1.52 software and values plotted into graphs.

2.9. Structural stability test via protease-heat combination

To learn of the unfolding kinetics of our protein and the structural stabilities of the various subunit domains that constitute the protein, we subjected samples of the protein to heat at 70 ˚C, or 80 ˚C in the absence of denaturants, and aliquots withdrawn and quenched at specified time points (0, 2.5, 5, 10, 15, 20, 30 and 60 min). A 1:20 w/w ratio of enzyme to EƐ34 TSP sample was used for the proteolytic process, enzyme digestion was allowed for 30 min, and quenching was achieved via mixing reaction samples with a protease inhibitor followed by the addition of SDS-free gel loading buffer consisting of 50 mM Tris-HCl, 25% glycerol, and 0.01% bromophenol blue, and SDS free running buffer consisting of 25 mM Tris-HCl, and 0.2 M glycine. Samples of triplicate experiments were electrophoresed for 60 min and stained with Coommasie blue, and then intensities of the bands generated recorded. The densitometric values were compiled from the three replicate experiments and averaged. The mean densitometric values for the 80 °C heating experiment were plotted against time of heating.

2.10. Decellularization of Avian articular cartilage as scaffold (DACS)

Thin sections of avian articular cartilages (500 µm) were treated with 0.1 mg/mL DNase, 0.05 mg/mL RNase final concentrations for 1 h, then the specimen decellularized using 1% SDS for 36 h. Cartilage tissue samples were microtomed to a thickness of 500 µm using HM315 Rotary Microtome (microm, Germany). Decellularization was carried out on a rocking platform (Variable Rocker, MIDSCI) under maximum rocking at room temperature. After decellularization, the cartilage specimens were washed 5 times with distilled water and then sterilized in 70% ethanol. Finally, the sterilant was removed.

2.11. Quantification of Biofilm formation

To investigate biofilm formation on the decellularized avian cartilage samples, we adopted a similar method as described by Li et al., 2010, and Li et al., 2021 **[40,41]** with few modifications. In summary, 400 µl of *S. newington* at an OD_{600} value of 0.2 was transferred to the well of a 24-well plate containing decellularized avian cartilage. After inoculation, samples were incubated at 37 °C for 36 h in MaxQ 4450 incubator (Thermo Scientific) without shaking, samples were washed with 1X PBS thrice, fixed in 10% formaldehyde, incubated with 0.2% SDS for permealization for 1 h and stained with Propidium Iodide (PI) Ready Flow™ Reagen (ThermoFisher Scientific, USA) at room temperature for 10 min. Afterwards, samples were washed under mild water flow and careful dried. Stained biofilms were dissolved in 25% acetic acid, and the absorbance was read using Evolution 350 UV-Vis spectrophotometer (Thermo Scientific). The experiment was repeated thrice. The replicate readings were averaged. Statistical analyses were carried out using student's t test, and p values of less than 0.05 were considered significant.

2.12. Immunofluorescent imaging of Biofilm formation

Preprints (www.preprints.org) | NOT PEER-REVIEWED | Posted: 21 October 2021 doi:10.20944/preprints202110.0308.v1

Specimen containing *S. newington* biofilm were washed with 1X PBS thrice fixed and permeabilized, then followed with incubation of specimen in 4′, 6-diamidino-2-phenylindole (DAPI) (ThermoFisher Scientific) solution and PI for 2 h at room temperature. Then, dye washed off with 1X PBS thrice and specimen imaged using EVOS FLC microscope (Life Technologies).

2.13. Scanning Electron Microscopy (SEM)

Sample preparation for SEM was carried out as described by Li et al., 2021 **[41]** with few modifications. In short, the specimens for SEM were fixed with 10% formaldehyde solution at room temperature for 10 min, washed with PBS solution thrice, and dehydrated serially in 50%, 70%, and 95% absolute ethanol solutions for 10 min each. Finally, the specimens were dried in a vacuum, and sprayed with gold using EMS Quorum (EMS 150R ES) ion-sputtering instrument and observed through Analytical Scanning Electron Microscope (SEM) (JEOL JSM-6010LA, Japan) installed with IntouchScope software.

2.14. Homology modeling of *S. newington* outer member protein A (ompA)

The **ompA** (GenBank ID: QIN18792.1) sequence was extracted from the NCBI website and subjected to homology modeling using the Swiss-Modeler (http://swiss-model.expasy.org/) program **[42-44]**. The *E. coli* outer membrane protein (PDB ID: 1bxw.1.A) **[45]** that share 91.18% amino acid sequence similarity to **ompA** was used as a template. The modeled structure is shown in **Figure 12**. To evaluate the model, it was subjected to Ramachandran plot analysis. The analysis showed a molprobity of 2.43 a clash score of 2.32, 86.63% Ramachandran favored structure, 6.98% Ramachandran outliers, 11.11% rotamer outliers and 1 bad bond out of 1377 bonds. The model scored a global quality estimate (QMEAN Global) of 0.66 ±0.07 (**See supplementary Figure 1**).

2.15. The complex contact prediction of Ɛ34 TSP to ompA, ompX and MIaD of *S. newington*

The interfacial contacts between two potentially interaction molecules can be predicted **[46-49].** The ComplexContact (http://raptorx2.uchicago.edu/ComplexContact/) web server was used for the sequence-based interfacial residue-residue contact prediction for the putative protein complex between Ɛ34 TSP and ompA of *S. newington* thus allowing full grasp of the Ɛ34 TSP-ompA interaction at residue level. The program work by searching for the sequence homologs between the two proteins and then creates paired multiple sequence alignments (MSA), then followed by applying co-evolution analysis and CASP-winning deep learning method to predict contacts **[50].** The predicted contacts are visualized as an image with darkened spot showing higher contact probability and lighter regions showing lower interfacial contact probability **[51]**. Amino acid sequences of Ɛ34 TSP (GenBank ID: 7353089), ompX (GenBank ID: QQJ27848.1), MIaD (GenBank ID: QQJ25883.1) and ompA (GenBank ID: QIN18792.1) in FASTA formats were submitted to the ComplexContact prediction tool of RAPTOR X program. Results consisting of the probabilities of interfacial contacts also indicated as darkened spots on an image were obtained. The residues of the two molecules that produced the highest probability in the complex contact prediction was picked as the interacting motifs and their probabilities averaged. The averaged values were exported to Excel (Microsoft, 2016) and plotted as a graph. The highest average probability (0.7381) corresponded with Ɛ34 TSP-ompA interaction at residue site G29-D39 (GKIYIGKIDTD) of Ɛ34 TSP and residues P132, G133, D141, F148 and I152 of ompA. The Ɛ34 TSP-MIaD contactcomplex prediction produced an averaged lower probability of 0.3065 whereas the Ɛ34 TSP-ompX recorded the lowest of 0.1984.

2.16. Molecular Docking analysis of Ɛ34 TSP- ompA of *S. newington*

The crystal structure of ompA of *S. newington* has yet to be determine as of date, hence the modeled structure of ompA of *S. newington* as described in section above was used for the docking analysis. The modeled 3D structure of ompA was docked to Ɛ34 TSP peptide G29-D39 (GKIYIGKIDTD) using PyRx (an open-source software for performing virtual screening that combines AutoDock Vina, AutoDock 4.2, Mayavi, Open Babel etc.**) [52-54].** The modeled structure of ompA served as the receptor molecule. The receptor was prepared using AutoDock Vina wizard, whereas the short peptide ligand (G29-D39 (GKIYIGKIDTD)) of Ɛ34 TSP was extracted using Biovia Discovery Studio software (version; 21.1.0.278) and prepared for docking using the Open Babel tool described similarly by our previous work **[55]**. Subsequently, the ligand structure was minimized and converted to a pdbqt format before uploading as a ligand. In the case of the ompA receptor, the bond orders were assigned, and charged hydrogen atoms added to the protein. The ompA receptor structure was also minimized using the AutoDock Vina wizard. The receptor grid box was generated in PyRx using the build-in Vina Wizard module, the grid box consisted of Vina search space of X: 6.03, Y: 28.60, Z: 32.70. The dimensions of the grid box were X: 35.12 Å, Y: 47.86Å, and Z: 45.93Å. AutoDocking of Ɛ34 TSP peptide to the ompA receptor was made by

Preprints (www.preprints.org) | NOT PEER-REVIEWED | Posted: 21 October 2021 doi:10.20944/preprints202110.0308.v1

using the AutoDock wizard in-built in PyRx program with an exhaustiveness of 8. The best ompA-Ɛ34 TSP peptide docked complex with highest relative free binding energy was saved as a pdb file and exported into Biovia Discovery Studio software for specific atomic-atomic interaction analysis between the ligand and the receptor.

Statistical analyses

For all statistical data, values were derived from multiple measurements (from replicates of 3 or 5 experiments) and averaged, the standard deviations were evaluated using P-values of Student's t-test (two-tailed, two samples of unequal variance, significance level $\alpha \geq 0.05$).

3. Results

3.1. Antibacterial effects of E34 phage, EE34 TSP and Vero cell culture supernatant

The antibacterial property of Ɛ34 phage, EƐ34 TSP and their combinations with Vero cell culture supernatant were investigated. As shown in **Figure 1A**, treatment of *S. newington* to EƐ34 TSP significantly reduced the growth of *S. newington* in all time points, however, the combination treatment of *S. newington* to EƐ34 TSP and V. Sup (**Figure 1C**) seems to demonstrate a complete elimination of the bacteria with increasing culturing time points. There were observed growth of *S. newington* with time for cells treated with Ɛ34 phage only (**Figure 1D**), or with Ɛ34 phage dilutions, however, in a combination treatment for which *S. newington* was treated with both Ɛ34 phage and V. Sup, there was drastic reduction in bacterial cell growth (**Figure 1B**).

Figure 1. Growth kinetics of *S. newington* treated with EƐ34 TSP (A), Ɛ34 phage –Vero cell culture supernatant (B), EƐ34 TSP–Vero cell culture supernatant (C), and Ɛ34 phage (D).

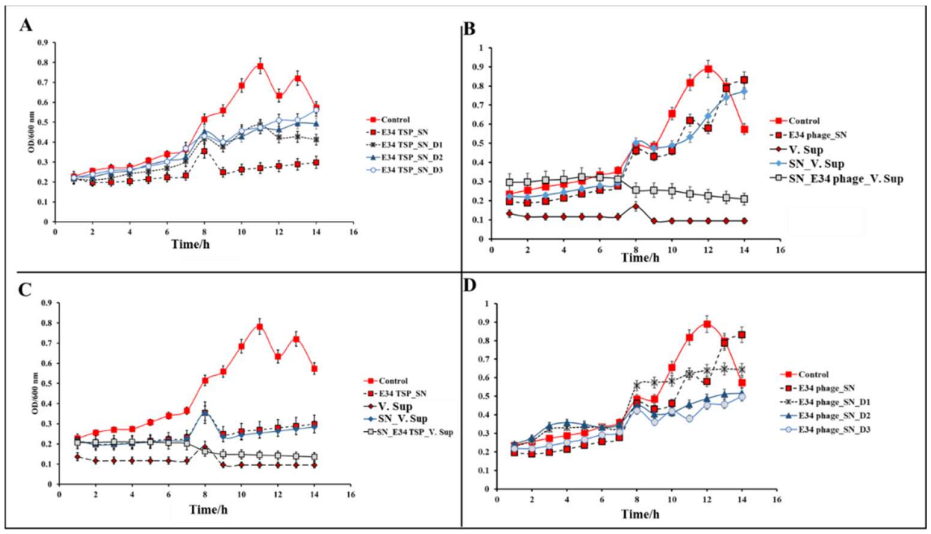

(A) Ɛ34 TSP_SN denotes EƐ34 TSP (390 µl/ml) treated *S. newington*. Ɛ34 TSP_SN_D1 denotes *S. newington* treated to dilution 1 of EƐ34 TSP (39.00 µg/ml). Ɛ34 TSP_SN_D2 denotes *S. newington* treated to dilution 2 of EƐ34 TSP (3.90 µg/ml). Ɛ34 TSP_SN_D3 denotes S. newington treated to dilution 3 of EƐ34 TSP (0.39 µg/ml). Ɛ34 TSP_SN_D2 denotes *S. newington* treated to dilution 2 of Ɛ34 TSP (3.9 µg/ml).

(B) Ɛ34 phage_SN denotes *S. newington* infected with Ɛ34 phage (MOI of 10). V. Sup denotes Vero cell culture supernatant only for which *S. newington* was not inoculated. SN _V. Sup denotes *S. newington* treated to V. cell culture supernatant. SN_Ɛ34 phage_V. Sup denotes a combination treatment of *S. newington* to Ɛ34 phage (MOI of 10) and Vero cell culture supernatant.

(C) Ɛ34 TSP_SN denotes the treatment of *S. newington* to EƐ34 TSP (390 µg/ml). V. Sup denotes Vero cell culture supernatant only for which *S. newington* was not inoculated. SN_Ɛ34 TSP_V. Sup denotes a combination treatment of *S. newington* to EƐ34 TSP (390 µg/ml) and Vero cell culture supernatant.

(D) Ɛ34 phage_SN denotes *S. newington* infected with Ɛ34 phage (MOI of 10). Ɛ34 phage_SN_D1 denotes treatment of *S. newington* to dilution 1 of Ɛ34 phage (MOI of 1). Ɛ34 phage_SN_D2 denotes treatment of *S. newington* to dilution 2 of Ɛ34 phage (MOI of 0.1).

Preprints (www.preprints.org) | NOT PEER-REVIEWED | Posted: 21 October 2021 doi:10.20944/preprints202110.0308.v1

Figure 2. Antibacterial potential of Ɛ34 phage and EƐ34 TSP **(A)** Comparative analysis of the EƐ34 TSP and Ɛ34 phages as antibacterial agents **(B)** Comparative analysis of the EƐ34 TSP-Vero cell supernatant and Ɛ34 phages –Vero cell supernatant as antibacterial agents.

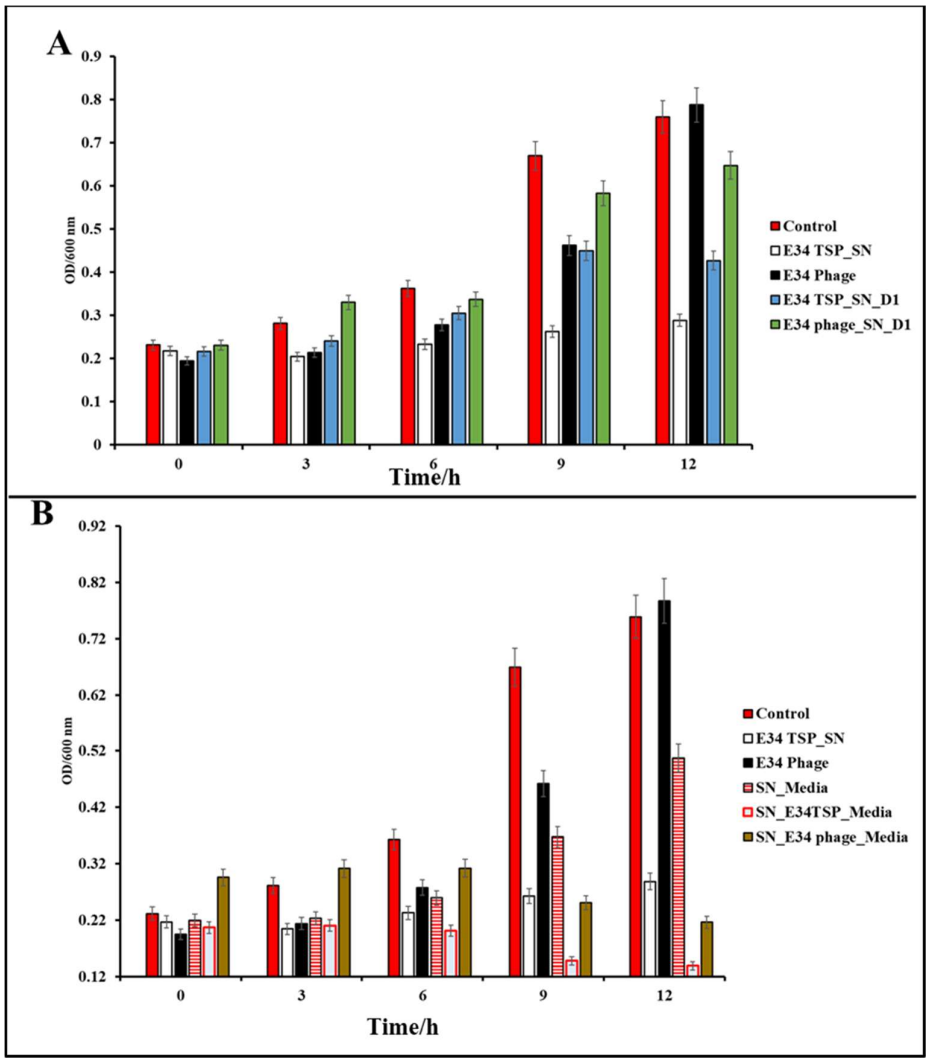

(A) Comparison of Ɛ34 phage and EƐ34 TSP treatment to *S. newington* in different time points. The optical densities readings were recorded at 600 nm for 3 replicates, and averages used to plot graph.

(B) Comparison of Ɛ34 phage –Vero cell culture supernatant combination treatment to *S. newington* against Ɛ34 TSP – Vero cell culture supernatant treatment to *S. newington* in different time points. The optical densities readings were recorded at 600 nm for 3 replicates, and averages used to plot graph.

As shown **Figure 2A,** an initial starting culture of 0.2 OD showed varied *S. newington* growth kinetics with increasing time points. While the control (1x PBS) and Ɛ34 phage (Ɛ34 phage_SN_D1) at MOI of 1 both showed steady growth kinetics, the Ɛ34 TSP (39 µl/ml) treated to *S. newington* (Ɛ34 TSP_SN_D1) showed lower growth kinetics compared to the phage treated samples. Ɛ34 phage (MO1 = 10) showed lower growths at the first 9 h time point of culture, but interestingly showed higher growth than Ɛ34 phage at MOI of 1 at the 12 h time point. The *S. newington* treated to Ɛ34 TSP at concentration of 390 µl/ml showed the lowest growth in all culturing time points.

As shown in **Figure 2B**, an initial starting culture of approximately 0.23 OD showed varied *S. newington* growth kinetics with increasing time points. While the control (1x PBS) and Ɛ34 phage (Ɛ34 phage_SN) at MOI of 10 both showed steady growth kinetics, the Ɛ34 TSP (390 µl/ml) treated to *S. newington* (Ɛ34 TSP_SN) showed very low growth in all time points. The slowest growth kinetics was observed to the combination treatment of

Preprints (www.preprints.org) | NOT PEER-REVIEWED | Posted: 21 October 2021 doi:10.20944/preprints202110.0308.v1

S. newington to Ɛ34 TSP (390 µl/ml) and Vero cell culture supernatant (V. Sup). Comparatively, the phage (MOI = 10) and V. Sup treated samples also recorded lower ODs in all culturing time points.

Figure 3. Spot test of antibacterial potency of EƐ34 TSP, Ɛ34 Phage, EƐ34 TSP-Vero cell culture supernatant (V. Sup), and Ɛ34 phage -V. Sup on *S. newington*

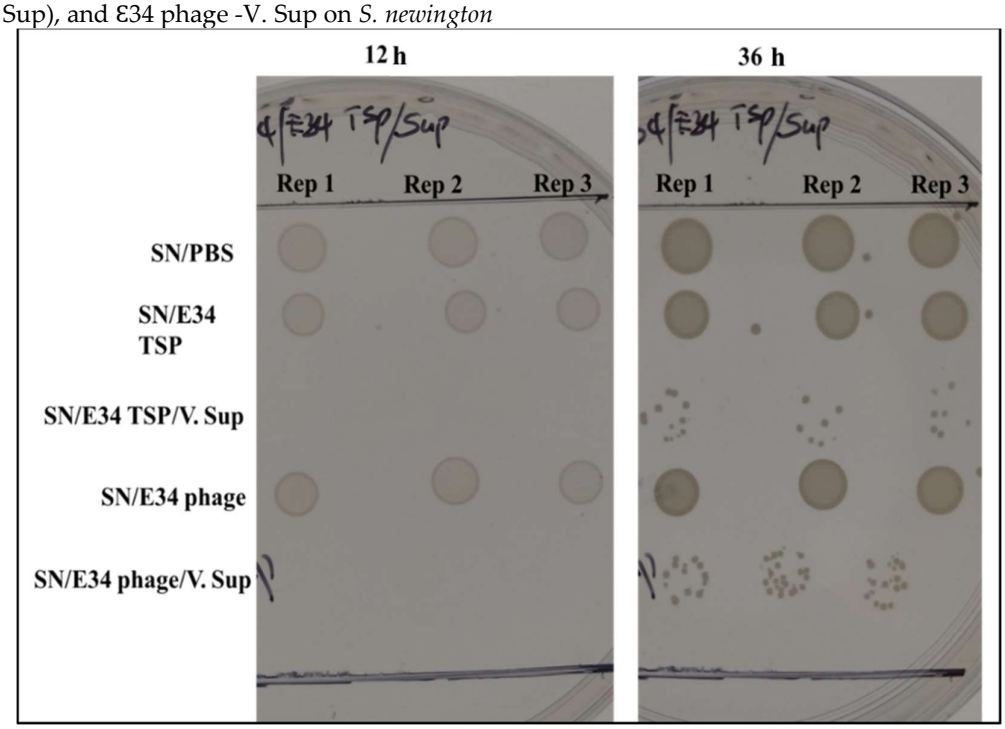

As shown in **Figure 3**, 10 µl aliquot from *S. newington* suspension at OD of 0.5 in LB broth was spotted on the surface of LB agar and quickly followed with same volume of EƐ34 TSP (390 µg/ml) or Ɛ34 phage solution (MOI = 1) or their combination with Vero cell culture supernatant. Agar plates were incubated for 12 and 24 h at 37 °C. The antibacterial activity was determined by the presence or absence of colony forming units formed after 12 h and 36 h time points. As shown, 12 SN/PBS which depicts *S. newington* in 1X PBS served as control, and spot showed growth of colonies at both 12 h and 36 h time points. SN/Ɛ34 TSP which depicts *S. newington* treatment to EƐ34 TSP showed growth in both, similar observation was recorded for *S. newington* treated with Ɛ34 phage (SN/Ɛ34 phage), however, when *S. newington* was treated to Ɛ34 TSP and Vero cell culture supernatant (SN/Ɛ34 TSP/V. Sup), there was no growth at 12 h time point, however an observed average of 7.33 colony forming units (CFUs) were recorded at the 36 h time point. Similarly, when *S. newington* was treated to Ɛ34 phage and Vero cell culture supernatant combination (SN/Ɛ34 phage/V. Sup), there was no observed growth at 12 h time point, but recorded few CFUs (14.00) at the 36 h time point.

3.2. EƐ34 TSP sensitivity to trypsin under non-denaturing conditions

Our data as shown in **Figure 3A** indicate that EƐ34 tsp untreated samples migrated as a blurry band in the native gel electrophoresis, which is a characteristic feature we have observed in all experiments with native electrophoretic analysis of EƐ34 TSP. The rEK digested samples (MƐ34) has been demonstrated to be resistant to trypsin as indicated on lane 3 **Figure 3A**. EƐ34 TSP treated to trypsin as shown in lanes 4 has these species migrating at the same level as the rEK cut samples (**Figure 3A, lane 3**), more so, they also seem to be exhibiting indistinguishable band pattern similarly to the rEK digested EƐ34 TSP. These two features observed seems to show the possibility of EƐ34 TSP sensitivity to trypsin via the 43 amino acid fusion peptides only. The undigested and untreated samples of the protein can be differentiated from the rEK digested as well as the trypsin treated EƐ34 TSP by their electrophoretic mobility. This indicates that the wild-type Ɛ34 TSP is resistant to trypsin, however, the fusion peptide placed n-terminally to the protein during the cloning process is sensitive to the enzyme.

Figure 3. Trypsin treatment of EƐ34 TSP and Matured Eɛ34 tsp at physiological temperature **(A)** EƐ34 TSP treated to trypsin without SDS **(B)** EƐ34 TSP treated to trypsin in 2% SDS.

Preprints (www.preprints.org) | NOT PEER-REVIEWED | Posted: 21 October 2021 doi:10.20944/preprints202110.0308.v1

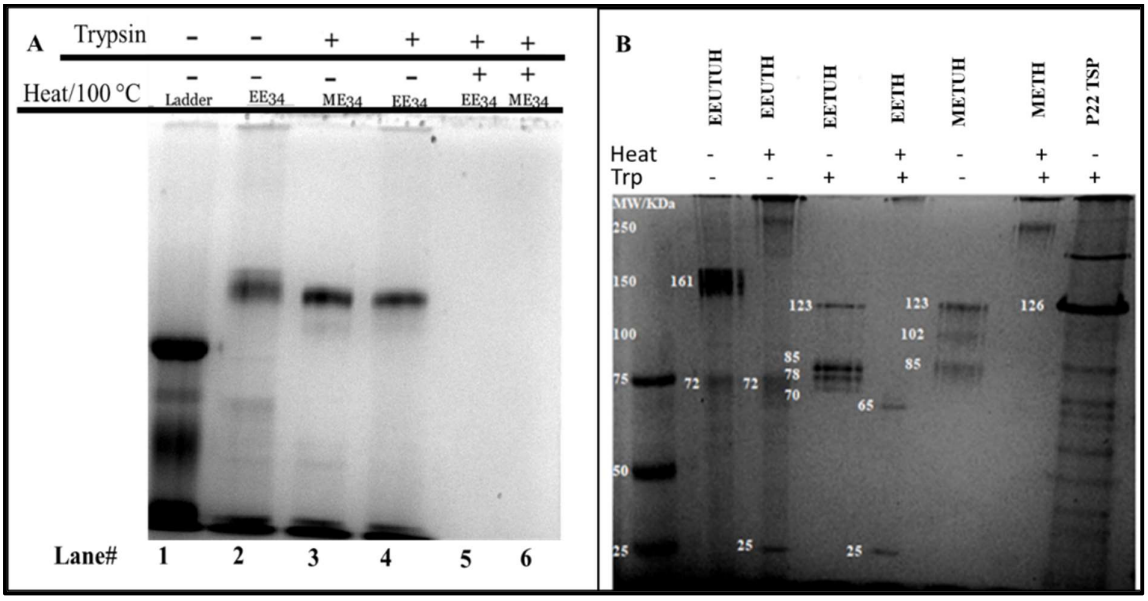

As shown in **Figure 3A**, trypsin treatment of EƐ34 TSP and Matured EƐ34 TSP (MƐ34) (same as recombinant enterokinase digested EƐ34 TSP) at physiological temperature for 6 h. Samples were treated with trypsin and quenched after 6 h incubation in a 37 ˚C set water bath. Quenching was achieved via the addition of trypsin inhibitor and samples analyzed via 7.5% Native-PAGE and visualized by Coommasie blue staining. The MƐ34 TSP migrated at the same molecular size as the EƐ34 TSP treated to trypsin, this might indicate that trypsin digestion only removed the 43 amino acid fusion peptide. Heated samples as in lane 4 and 6 showed no bands, indicative of complete proteolysis.

As shown in **Figure 3B**, 0.5 mg/ml of EƐ34 TSP and MƐ34 TSP were dialyzed, then mixed with 0.2% SDS followed by treatment to trypsin at 1:20 w/w of enzyme to protein. The treated samples were then incubated in water bath at 37 ˚C for 6 h. Proteolytic reactions were stopped by the addition of protease inhibitor 10 µg/ml final concentration, then electrophoretically analyzed using 10% polyacrylamide gel.

3.3. EƐ34 TSP sensitivity to Enzymes (trypsin or PK) under 2% SDS at physiological temperature

3.3.1. Partial sensitivity of EƐ34 TSP in 2% SDS to trypsin

In this study, EƐ34 TSP showed partial susceptibility to trypsin in similar fashion to that of TSP3 of Greenfield et al., 2019 **[56]**. Treating extended Ɛ34 TSP (EƐ34 TSP) in 2% SDS to trypsin at 37 ˚C for 6 h yielded four protein products (**Figure 3B, lane EETUH**) labeled 123, 85, 78 and 70 KDa respectively. The 123 KDa fragment corresponded to the size of the MƐ34 TSP (that is when EƐ34 TSP has the extra 43 amino acid cleaved by recombinant Enterokinase (rEK)). And while the 85, 78 and 70 KDa fragments might indicate proteolytic cleavage of our protein at sites other than the fusion peptide. As a control, MƐ34 TSP (rEK digested EƐ34 TSP) was treated to trypsin for same period and loaded onto a 7.5% polyacrylamide gel and electrophoresed. Three protein fragments were recorded, the first corresponding to the normal size of the trimeric native Ɛ34 TSP of 123 KDa on the gel (but a 196.5KDa in actual calculated molecular weight), the two other fragments migrated at 102 and 85 KDa respectively (**Figure 3B**, lane METUH). P22 TSP was also treated with trypsin in the presence of 2% SDS, migrated at 126 KDa size, which corresponds to 215 KDa size of the P22 TSP trimer in actual calculated molecular weight. Similar reports of migration characteristics of the trimeric protein of P22 in a 7.5% polyacrylamide gel has been published by X. Carbonell and A. Villaverde, indicating a 126±3 KDa migration in gel but an actual size of 215 KDa **[57]**. As depicted in **Figure 3B,** EEUTUH (the extended Ɛ34 TSP untreated and unheated) recorded the trimeric species migrating at blurry consistency at averagely 161 KDa. The untreated but heated (EEUTH) sample as in third lane recorded a single band as expected and migrated at 72 KDa indicative of complete unfolding to monomers after heating. As shown in the fourth lane of **Figure 3B,** four protein fragments bands were recorded when EƐ34 TSP in 2% SDS was treated with trypsin for the 6 h time period. The first band was recorded at 123 KDa, the three other fragments migrated at 85 KDa, 78 KDa and 70 KDa respectively. In the firth lane, the EƐ34 TSP samples which received treatment to trypsin for 6 h were then subjected to unfolding

Preprints (www.preprints.org) | NOT PEER-REVIEWED | Posted: 21 October 2021 doi:10.20944/preprints202110.0308.v1

via heat at 100 °C for 5 min, these treated and heated (EETH) samples produced two bands, a larger fragment migrating at 65 KDa, and a smaller one migrating at 25 KDa. MƐ34 TSP treated to trypsin in the presence of 2% SDS for 6 h produced three fragments, the first fragment was observed at the 123 KDa size, indicating no proteolysis, the two other fragments migrated at 102 KDa, and 82 KDa, indicative of sensitivity of some of the species of the MƐ34 TSP to the enzyme. P22 TSP was also treated with trypsin as shown in eighth lane of same **Figure 3B**. A single band was observed at 126 KDa, which corresponds to 215 KDa size of the P22 TSP trimer in actual calculated molecular weight similar to reports by Carbonell and Villaverde **[58]**.

A comparison of the migration between MƐ34, the trypsin treated EƐ34 TSP hints a positive correlation in molecular weights, with both species migrating at 123 KDa in the 7.5% polyacrylamide gel corresponding to 196.5 KDa in calculated molecular weight. The untreated EƐ34 TSP, however, in its trimeric state migrated as a blurry band (averaging 161 KDa size). The theoretical molecular weight of the EƐ34 TSP is calculated to be 214 KDa, which represents a homotrimer made from the three monomers (each monomer is made of 649 amino acids) (that is, the native protein which consist of 606 amino acids and the 43 amino acids coming from the fusion peptide). When the trypsin treated EƐ34 TSP samples were heat denatured to reveal the monomeric size of the proteolytic products, two bands were observed on the 7.5% gel. Of these two bands, one band migrated at 65KDa, and the second fragment band migrated at the 25 KDa size.

Even though it is insufficient to draw any strong generalization, notwithstanding, it is worth noting that the calculated molecular weight of MƐ34 TSP monomer without the fusion peptide is 65.5KDa, hinting a similar size as the proteolytic fragment at the 65 KDa migration monomer recorded as in the fifth lane of **Figure 3B**. The 25 KDa fragment observed might represent the unfolded state of the proteolytic fragments of the 85, 78 and 70 KDa proteins (**Figure 3B**; EETUH). The three other protein fragment bands which migrated at 85, 78 and 70 KDa respectively, might have migrated differently due to sterical differences in conformation after proteolysis or due to cleavages at several different sites by trypsin. These findings suggest that tryptic digest of EƐ34 TSP in the presence of 2% SDS might have cleaved the fusion peptide at the N-terminal region leaving the native Ɛ34 TSP fully intact at first, however extended time of incubation in the denaturing condition partially unfolded the protein to cause trypsin to bind to and cleave previously solvent inaccessible regions.

Figure 4. **(A)** Enzymatic digestion of EƐ34 TSP in varying concentrations of Trypsin **(B)** Diagrammatical illustration of the possible pattern of proteolysis with heat unfolding of protein followed with enzyme treatment.

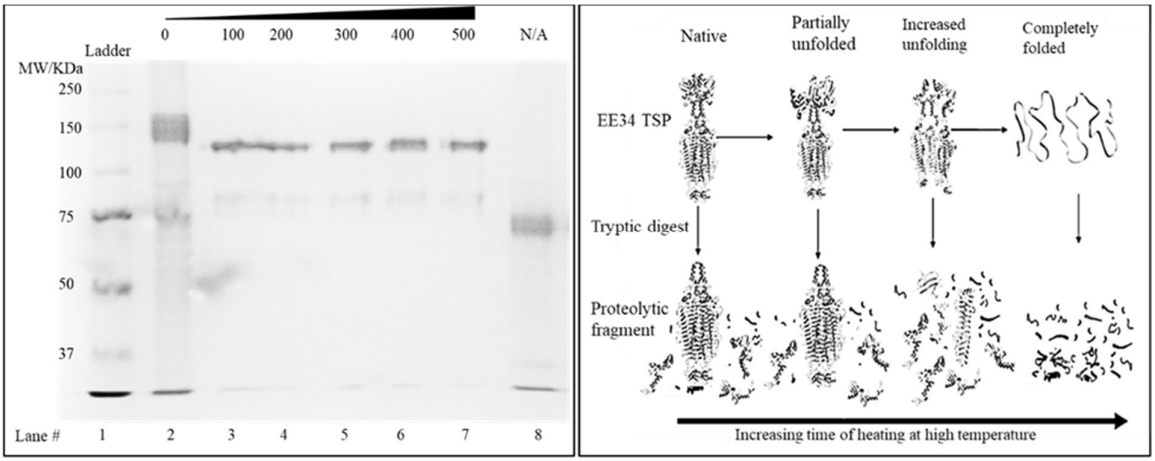

EƐ34 TSP digestion under varying concentration of trypsin. Samples were run in 7.5% Native PAGE. As shown in **Figure 4A**, 1 mg/ml of EƐ34 TSP each were subjected to varying concentration of trypsin digest for 6 h under 37 °C. There was no observed difference between different concentrations of trypsin treatment. Lane 1, Ladder (Prestained Precision Protein Standard). Lane 2, EƐ34 TSP; unheated and untreated. Lane 3, EƐ34 TSP; treated with 100 μg of trypsin. Lane 4, EƐ34 TSP treated with 200 μg of trypsin. Lane 5, EƐ34 TSP treated with 300 μg of trypsin. Lane 6, EƐ34 TSP treated with 400 μg of trypsin, Lane 7, EƐ34 TSP; treated with 500 μg of trypsin. Lane 8, EƐ34 TSP heated and untreated. Lane 9, EƐ34 TSP heated and untreated. Lane 10, blank.

Preprints (www.preprints.org) | NOT PEER-REVIEWED | Posted: 21 October 2021 doi:10.20944/preprints202110.0308.v1

Figure 4B. Cartooned representation of structural changes due to heat, and proteolytic events due to protease treatment. At room temperature, under non-denaturing buffer conditions and neutral pH, the majority of EƐ34 TSP species exist in solution as native trimers. However, when temperature is increased to unfold the protein, previously buried hydrophobic regions are exposed and easily attacked by protease hence leading to the degradation of the protein.

3.3.2. Enzymatic digestion of EƐ34 TSP to increasing concentration of trypsin (Qualitative)

Dose dependent tryptic proteolysis of EƐ34 TSP at 37 ˚C of EƐ34 TSP to trypsin as shown in **Figure 4A,** generated two bands each, representing two fragments produced from the proteolytic cleavage of the protein with trypsin; an upper denser band that migrates slightly below the native trimer of the EƐ34 TSP and a lower fainter band as seen in lanes 3 to 7 (**Figure 4A**). These upper bands match the 123 KDa migration as previously recorded (**Figure 3A,** lanes 3 and 4). This seems to point at a proteolytic digest of the 43 amino acid fusion peptide and leaving the full matured TSP intact. Another noticeable observation was the absence of any increase or decrease in band intensities in all concentrations of trypsin treatments. The second fragment band migrated at 77 KDa, whilst the first fragment band migrated at 123 KDa. We infer that the 123 KDa arouse from a proteolytic event that degraded the 43 amino acid whereas the 77 KDa fragment might come from less stable species of EƐ34 TSP that possibly had the last 70-60 amino acid of their C-termini truncated along with the 43 amino acid fusion peptide. We hypothesized that the second fragment bands might have been produced due to the long exposure of the protein to trypsin (6 h) hence rendering less stable species in the samples to unfold slightly, thereby enabling trypsin to bind and cleave them.

3.3.3. Probing the structural stability using heat-protease combination

In native state, most enzymes sites of the protein are shielded and inaccessible, thereby imparting resistance, however, if there exist structural domains that are flexible, or linker regions that are solvent accessible, these areas can easily be attacked by the enzymes leading to specific cleavages and production of truncated products with unique electrophoretic mobility. Our approach here was to unfold the native EƐ34 TSP while exposing it to trypsin. The EƐ34 TSP was subjected to gradual denaturation via heating at 70 ˚C and 80 ˚C for specified time points and aliquots withdrawn at these time points and treated with trypsin for 30 min. Thus, higher structure information such as thermostable domains could be deciphered and their stability against heat as well as unfolding rates of the truncated products revealed. This method also possesses the discretionary ability to detect from the onset species that were less stable and existing in non-native conformation.

3.3.4. EƐ34 TSP digestion at 70 ˚C using trypsin

As depicted in **Figure 6A**, the unfolding kinetics of EƐ34 TSP heated at 70 ˚C with the concomitant treatment of the heated protein to trypsin after briefly cooling to room temperature, showed similar band intensities for all treated samples from the 0 min to the 30 min. All treated samples migrated as single band in contrast to the blurry pattern recorded for the untreated samples (lane 2, **Figure 6A**). The data further suggests that EƐ34 TSP is resistant to trypsin even after heating at 70 ˚C.

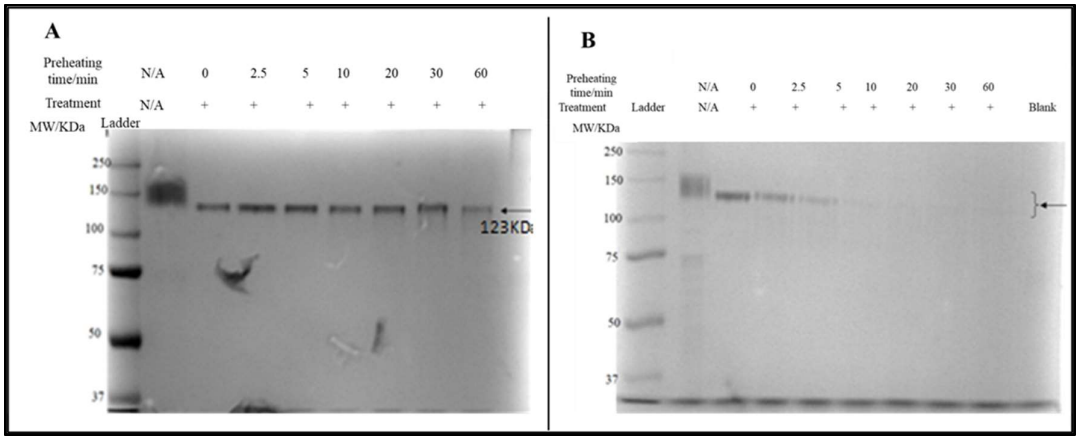

Figure 6. Treating EƐ34 TSP to trypsin after heating at high temperatures. **(A)** Treating EƐ34 TSP to trypsin after heating at 70 ˚C. **(B)** Treating EƐ34 TSP to trypsin after heating at 80 ˚C.

Preprints (www.preprints.org) | NOT PEER-REVIEWED | Posted: 21 October 2021 doi:10.20944/preprints202110.0308.v1

Figure 6 A. 0.5 mg/ml of EƐ34 TSP samples were heated at 70 ˚C. Heating of samples were done without the addition of SDS. Samples were withdrawn at set time points 0, 2.5, 5, 10, 15, 20, 30 and 60 min, then cooled briefly and subjected to tryptic digest. A ratio of 1:20 w/w of enzyme to EƐ34 TSP sample was used and the proteolytic reaction allowed to proceed for 6 h under 37 ˚C. Afterward, samples were electrophoretically analyzed in a 10% polyacrylamide gel under non denaturing conditions. **Figure 6A**: Lane 1, Ladder (Prestained Precision Protein Standard). Lane 2, EƐ34 TSP; unheated and untreated (EƐ34UHUT). Lane 3 to lane 9 received treatments from the 0, 2.5, 5, 10, 20, 30, and 60 min time points treatment samples of EƐ34 TSP respectively. **Figure 6B.** The same treatment process and lane labeling was repeated except an increase in temperature to 80 °C.

3.4.2 EƐ34 TSP digestion at 80 ˚C using trypsin

The proteolytic fragments as shown in lanes 0 to 60 min (**Figure 6B**) migrated at 123 KDa which represents the trimeric state of the protein. Observable also is the continual decrease in intensities of these bands with time. As can be seen, lane 0 is shown to possess higher band intensity than the fragment band in lane 2.5, and this disappearance of band intensities continued until nothing can be seen at lane 20, 30 and 60 (**Figure 6B**).

3.4.3 Quantitative assessment of unfolding kinetics of EƐ34 tsp at 80 ˚C via trypsin treatment

P22 TSP is shown to be highly resistant to heat, even at elevated temperatures, with Tm of 88 ˚C **[59]**, in this study, we investigated the thermo-stability and protease resistance of EƐ34 TSP at 80 ˚C. The structural elements of EƐ34 TSP share huge similarities to P22 TSP, for instance, both trimeric proteins possess a known highly stable parallel beta-helix domain **[60]**. With these similarities, could the two proteins possess similar unfolding kinetics at elevated temperatures? To answer this, we quantitatively assessed the unfolding rate of EƐ34 TSP by measuring the densitometric values of EƐ34 TSP bands after heating at 80 °C then followed with tryptic digest. Triplicate experiments were averaged, and values plotted on a graph as shown in **Figure 7**. The averages of the densitometric values recorded showed that, at time point 0, 99.63 densitometric mean value was recorded; after 2.5 min, a drop of approximately 9 points was observed as the densitometric value registered 90.87. A continued downward trajectory of densitometric mean values were observed for 5, 10, 20, 30 and 60 min, registering densitometric mean values of 65.61, 49.32, 34.44, 18.27 and 1.16 respectively. These data fitted a regression curve with the equation; $[f_t] = [f_0]e^{(-kt)}$ Where $[f_t]$ = fragment band intensity at time t, which could possibly also equate to the concentration of species of EƐ34 TSP still maintaining their trimeric states after t time of heating at 80 ˚C. $[f_0]$ = fragment band intensity produced after treatment with trypsin at the 0-time point; the time point at which no heat has been applied to the protein. e = mathematical constant = 2.72, k = 0.072, the rate of proteolytic degradation of EƐ34 TSP, which is positively correlated to the rate of unfolding of the TSP. The unfolding rate of EƐ34 TSP shown here is several folds higher than the unfolding rates observed in the P22 system, although with a slightly difference methods **[61-63]**.

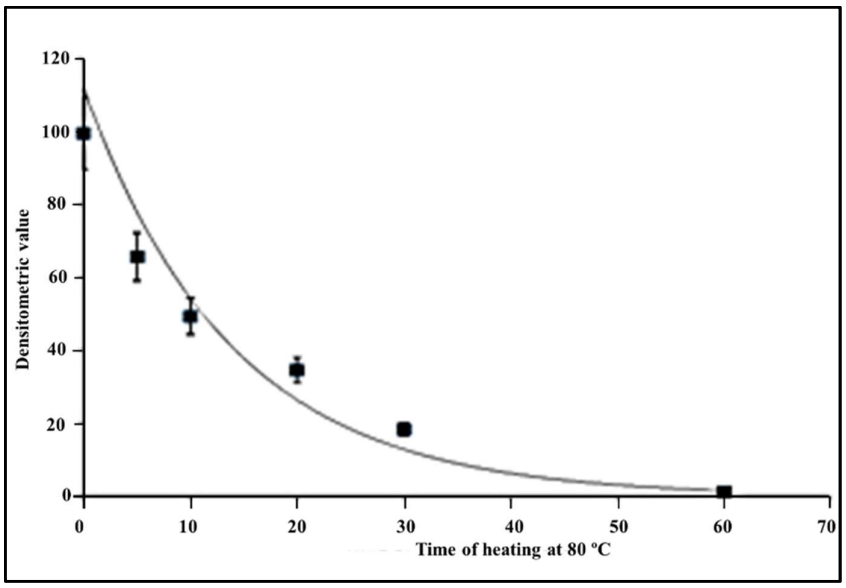

Figure 7. Quantitative assessment of unfolding kinetics of EƐ34 TSP at 80 ˚C via trypsin treatment

Preprints (www.preprints.org) | NOT PEER-REVIEWED | Posted: 21 October 2021 doi:10.20944/preprints202110.0308.v1

0.5 mg/ml of EƐ34 TSP samples were heated at 80 ˚C (**Figure 7**). Heating of samples were done without the addition of any denaturant. Samples were withdrawn at set time points 0, 2.5, 5, 10, 15, 20, 30 and 60 min, then cooled briefly and subjected to tryptic digest. A ratio of 1:20 w/w of enzyme to EƐ34 TSP sample was used and the proteolytic reaction allowed to proceed for 60 min under 37 ˚C. Afterward, samples were electrophoretically analyzed in a 10% polyacrylamide gel under non denaturing conditions. Gels were photographed (ChemiDoc XRS) and the densitometric values were acquired using Quantity one software. Triplicate experimental values were averaged and used to plot the chart. Data presented as mean ± SEM.

3.5 Biofilm inhibition

Biofilm-derived antibiotic tolerance of pathogenic bacteria remain a serious health issue **[64,65]**. Research into finding agents that inhibit biofilm formation is crucial. This can be accomplished by preventing the initial step of biofilm formation process, which is bacteria adhesion **[66]**. Secondly, bacteria depend majorly on quorum sensing in establishing biofilm, hence the ability to disrupt their quorum-sensing system will significantly enhance biofilm inhibition **[67,68].** Chemical agents that directly degrade biofilms have been investigated **[69]**, these agents can degrade or disrupt biofilm formation, however, most of these agents are not biocompatible. The application of phage therapy in biofilm prevention and control **[70]** are innovative alternatives that are also biocompatible. While the phage-host interaction usually determines the interaction of phages and host biofilm **[71]**, there are certain phages that directly degrades biofilm matrices **[72,73]**. Tkhilaishvili et al, 2018 showed that Sb-1 phage degrades the MRSA biofilm by digesting the exopolysaccharide component of the matrix. They also indicated that Sb-1 kills persisters either directly or by a Trojan horse effect **[74]**. The exposure of gram-negative bacteria to human or animal serum have been demonstrated to cause bactericidal activity **[75]**. The killing process is known to be orchestrated by the insertion into the bacterial envelope the activated complement components that attack the bacterial envelope via the membrane attack complex, which is activated via either the classical or the alternative pathway **[76,77]**. Other bacterial killing methods are the presence of antibacterial peptides in serum **[78]**. Yet again, bacteria have developed resistance to serum killing. Bacterial development of resistance against animal serum has been blamed on attainment of specific resistant genes, for instance, the ability of *E. coli* to survive exposure to 50% normal rabbit serum was found to correlate with the traT gene (80% of the serum resistant isolates were traT^{+}) **[79].** In this work, we investigated the ability of Vero cell supernatant to synergistically kill *S. newington* when combined with Ɛ34 phage or the fusion protein derived from this phage (EƐ34 TSP) (**Figure 1**). We also investigated this combined treatment method against *S. newington* biofilm formation (**Figure 8 and 9**). It was found that combinational treatment of *S. newington* with either phage and Vero cell culture supernatant, or the EƐ34 TSP and Vero cell culture supernatant significantly eradicated *S. newington* or its biofilm (**Figure 1, 8 and 9**). Employing scanning electron microscopy, we verified that decellularized avian cartilage treated to EƐ34 TSP and Vero cell culture combination, followed by inoculation of *S. newington* did not form significant amount of biofilm, whereas the untreated controls surfaces were covered by biofilm in 36 h time period (**Figure 10**).

Preprints (www.preprints.org) | NOT PEER-REVIEWED | Posted: 21 October 2021 doi:10.20944/preprints202110.0308.v1

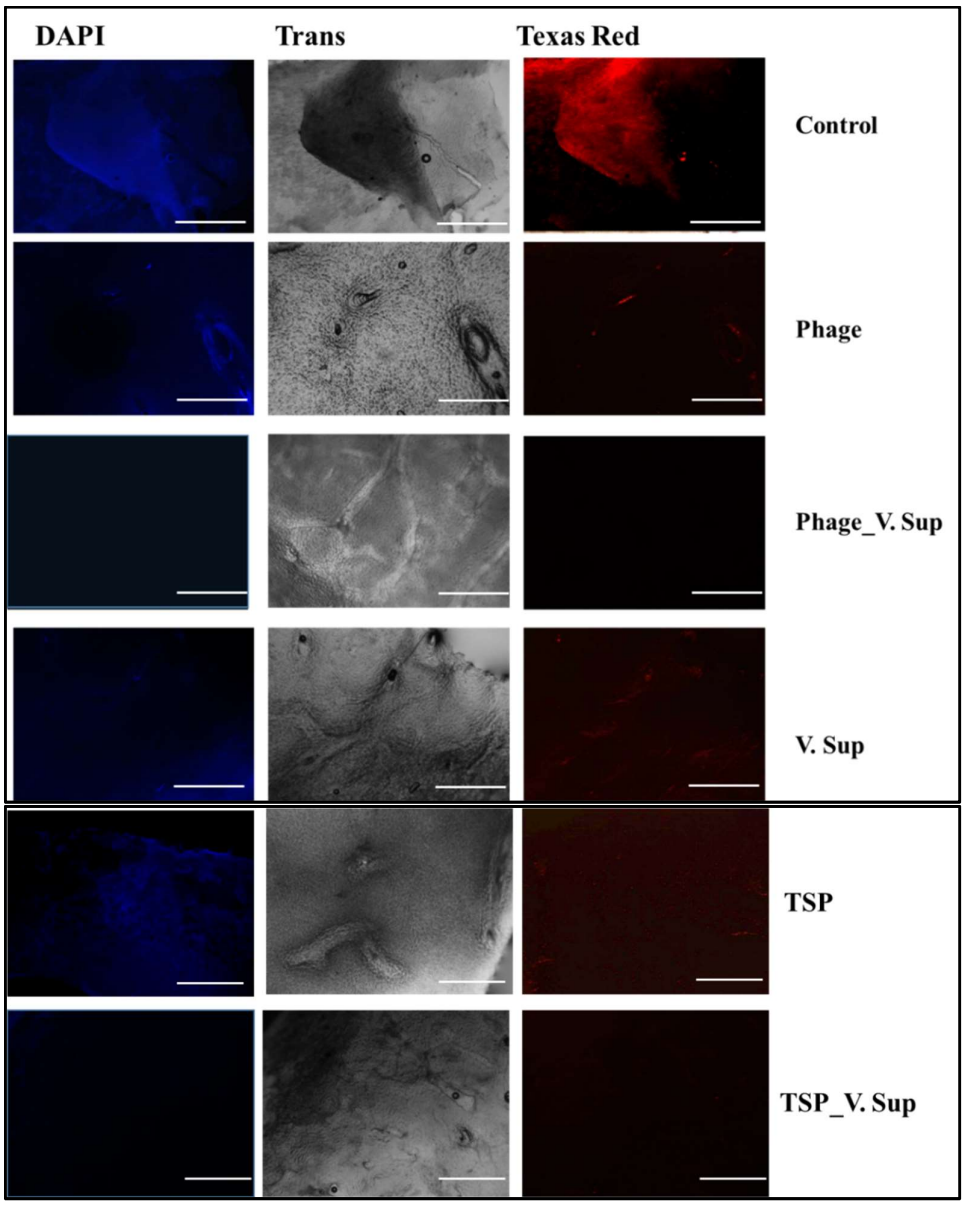

Figure 8. Immunostaining of biofilm formation on decellularized avian cartilage scaffold. Ɛ34 phage and Vero cell culture supernatant (Phage_V. sup) or EƐ34 TSP and Vero cell culture supernatant (TSP_V. sup) combination treatment significantly reduced the amount of biofilm formed by *S. newington* on decellularized avian cartilage. Control group showed the highest amount of biofilm formed as depicted by the high PI stain. TSP_V. sup and phage_V. sup showed the lowest PI stain indicative of less accumulation of biofilm. The DAPI stain in blue also corroborate with the findings of the PI staining. Scale bar = 500 μm.

Preprints (www.preprints.org) | NOT PEER-REVIEWED | Posted: 21 October 2021 doi:10.20944/preprints202110.0308.v1

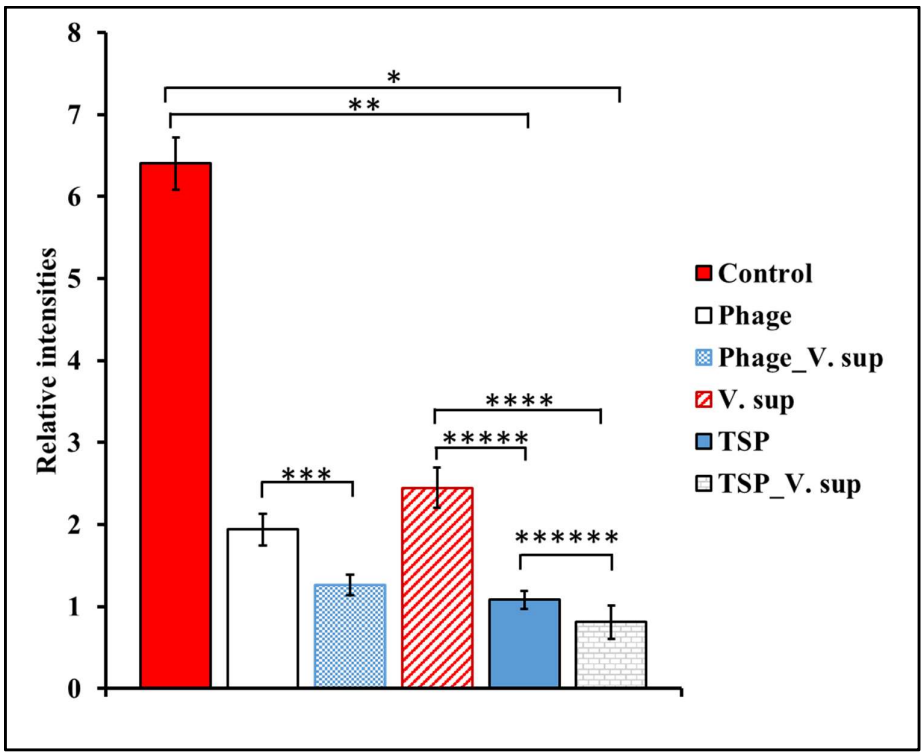

Figure 9. Biofilm inhibition by Ɛ34 phage and EƐ34 TSP in combination with Vero cell culture supernatant. *, **, ***, ****, *****, ******p values = 0.01, 0.01, 0.05, 0.01, 0.05 and 0.1 respectively.

The ability of Ɛ34 phage, Ɛ34 phage_V. sup, EƐ34 TSP, or EƐ34 TSP_V. Sup to inhibit the formation of biofilm on decellularized avian scaffold was studied. 400 µl of *S. newington* at an OD600 value of 0.2 was transferred to the well of a 24-well plate containing decellularized avian cartilage. Samples were incubated at 37 °C for 36 h in MaxQ 4450 incubator (Thermo Scientific) without shaking, samples were washed with 1X PBS thrice, fixed in 10% formaldehyde, incubated with 0.2% SDS for permealization for 1 h and stained with Propidium Iodide (PI) Ready Flow™ Reagent (ThermoFisher Scientific, USA) at room temperature for 10 min. Afterwards, samples were washed under mild water flow and careful dried. Stained biofilms were dissolved in 25% acetic acid, and the absorbance was read at 617 nm using Evolution 350 UV-Vis spectrophotometer (Thermo Scientific). The experiment was repeated thrice. The reading replicates were averaged. Statistical analyses were carried out using Student's t test, and p values of less than 0.05 were considered significant.

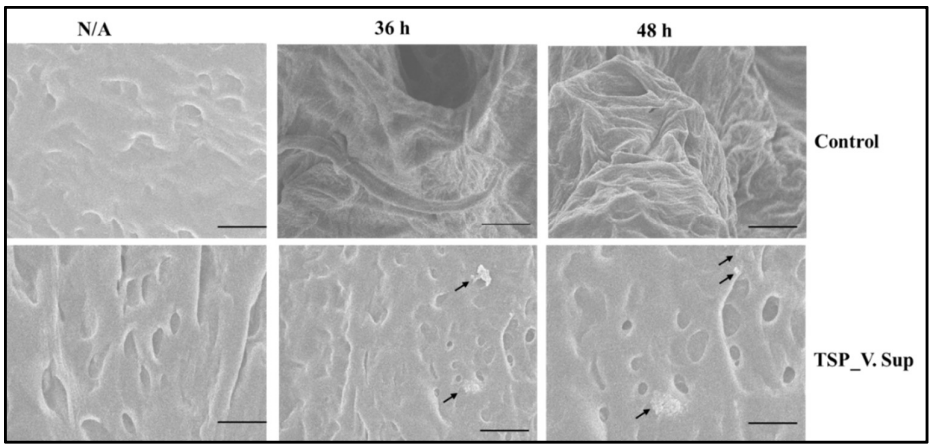

Figure 10. SEM images of biofilm formation on untreated control and Ɛ34 TSP and Vero cell culture supernatant combination treated decellularized avian cartilage scaffolds. Scale bar = 20 µm.

Preprints (www.preprints.org) | NOT PEER-REVIEWED | Posted: 21 October 2021 doi:10.20944/preprints202110.0308.v1

The decellularizing process removes chondrocytes from the cartilage tissue leaving behind an intact extracellular matrix with empty pores as shown in N/A column and most of the images of the TSP_V. sup row. However, upon *S. newington* inoculation and incubation, biofilm is formed, covering the surface of the control samples, whereas the TSP_V. sup samples remains mostly unaffected. Insignificant amount of biofilm deposits however can be seen on the TSP_V. sup samples as indicated by the black arrows on both 36 and 48 h time points. The washing process before fixing removed planktonic bacteria leaving the intact pores still visible, whereas the washing process in the control had no effect in removing the biofilm established by *S. newington*.

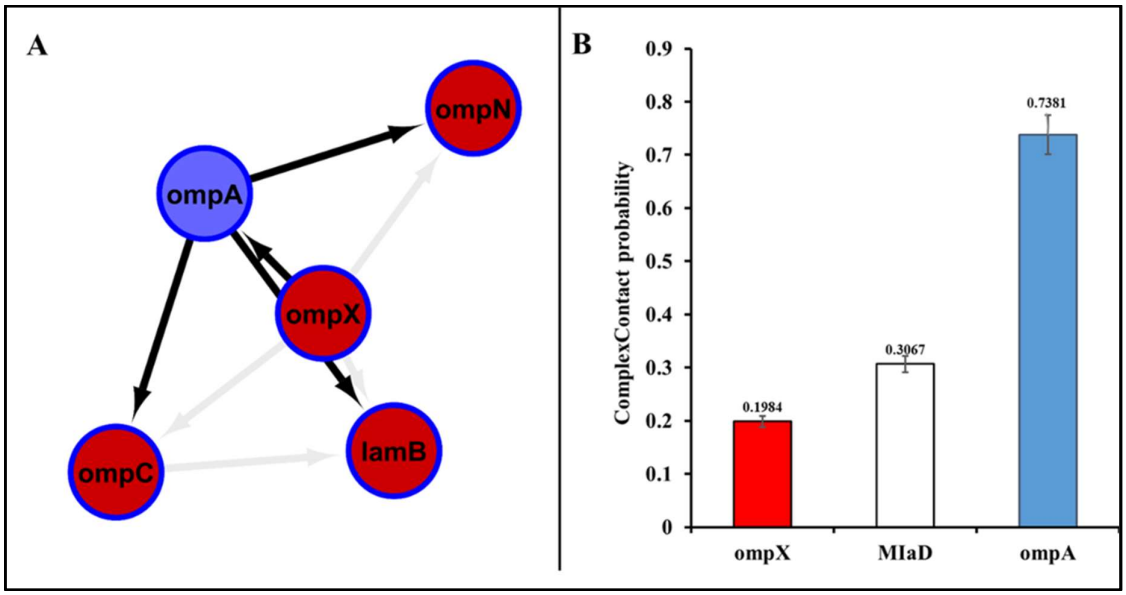

Figure 11. The outer membrane proteins of *S. newington* and their putative interactions. **(A)** STITCH Network of ompA. As shown, *Salmonella* ompA interacts directly with ompC, ompN, ompX and lamb. Networks derived by automated computational analysis using Cytoscape 3.8,2. **(B)** Complexcontact probabilities of ompX, MIaD and ompA with Ɛ34 TSP. Complexcontact probabilities values were acquired from ComplexContact (a web server for inter-protein contact prediction using deep learning) **[80]**.

As shown in **Figure 11A**, ompA interacts with ompX, ompN, ompC and lamB. OmpX is the outer membrane protease and is has been shown to be involved in cell adhesion. Its structure is an eight-stranded antiparallel beta-barrel that projects from the cell surface. Studies have shown that mutating this gene increase cell-surface contact in fimbriated strains but decrease contact in nonfimbriated strains **[81-84].** OmpA is the outer membrane protein A **[85-87]** which is a porin, responsible for diffusion of nonspecific small solutes across the outer membrane. In *E. coli*, this integral protein is implicated in phage adsorption, it is also a mediator of F-factor dependent conjugation. It is shown to be important in maintaining the structural shape of the outer membrane. The ompN also known as ompS2 is a Porin **[88];** which is allows ions and hydrophilic solutes to cross the outer membrane. MiaD is a member of the porin LamB family, it is a maltose-inducible porin which is involved in the transport of maltose and maltodextrins **[89-93].** OmpC is the outer membrane protein C, which belongs to the Gram-negative porin family **[94].**

Preprints (www.preprints.org) | NOT PEER-REVIEWED | Posted: 21 October 2021 doi:10.20944/preprints202110.0308.v1

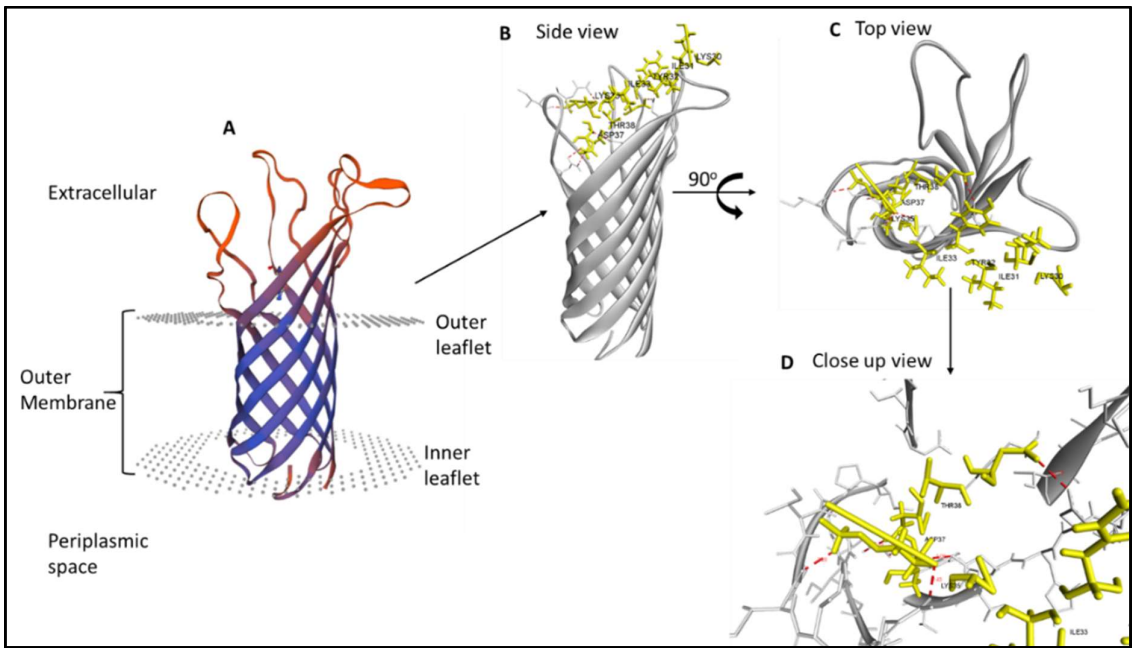

Figure 12. Molecular interaction of putative ompA with the N-terminal domain of Ɛ34 TSP. **(A)** Modeled structure of *S. newington* ompA (grey) (3D structure modeled using Swiss modeler web tool). **(B)** Side view of N-terminal epitope of Ɛ34 TSP (yellow), G29-D39, (GKIYIGKIDTD) in complex with the extracellular domain of ompA of *S. newington*. **(C)** Top view of the N-terminal epitope of Ɛ34 TSP in complex with the extracellular domain of ompA of *S. newington*. **(D)** Close up top view of N-terminal epitope in complex with the extracellular domain of ompA of *S. newington* (Docking analysis was carried out using PyRx molecular docking software). The short peptide of the Ɛ34 TSP bonded with ompA via the following residues; ILE36 of the peptide formed a hydrogen bond with ASP141 of ompA with a bond distance of 3.05Å. LYS35 of the peptide bonded with ILE178 of ompA (bond distance; 2.28Å). ASP39 of the peptide bonded with ASP139 (bond distance; 2.70Å). ASP37 bonded with ASN171 (bond distance; 2.89Å). ASN176 bonded with LYS35 (bond distance; 2.433Å). Finally, ASN171 bonded with ASP37 (bond distance; 2.44Å). The bonds were record as hydrogen bonds, thus producing a high affinity with relative free energy of -11.3 kcal/mol. Such free energy almost doubled the amount recorded in our previous docking analysis of Ɛ34 TSP interaction with the LPS of *S. newington* (which recorded -6.4kcal/mol).

Discussion

The antibacterial property of Ɛ34 phage, EƐ34 TSP and their combinations with Vero cell culture supernatant were investigated. While the phage employs the lytic process in killing *S. newington*, the mode of killing of *S. newington* mediated by EƐ34 TSP is currently unknown. As shown in **Figure 1A**, treatment of *S. newington* to EƐ34 TSP significantly reduced the growth of *S. newington* in all time points. Additionally, the combination treatment of *S. newington* to EƐ34 TSP and V. Sup (**Figure 1C**) seems to demonstrate a complete elimination of the bacteria with increasing culturing time points. There were observed growth of *S. newington* with time for cells treated with Ɛ34 phage only (**Figure 1D**), or with Ɛ34 phage dilutions, however, in a combination treatment for which *S. newington* was treated with both Ɛ34 phage and V. Sup, there was drastic reduction in bacterial cell growth (**Figure 1B**). We hypothesize that EƐ34 interacts and binds the ompA with its free N-terminal domain (serving as a "latch"). Whereas the receptor binding domain (RBD) recognizes and binds to LPS of *S. newington*. The binding and processivity of the RBD might provide the "tugging" force to pull and disrupt the ompA receptor. This argument seems to corroborate with our *in silico* analysis that shows that the RBD of Ɛ34 TSP bindings to ompA with a high probability of 0.7318 (**Figure 10**) and a relative free binding energy of -11.3kcal/mol. Additionally, the proteolytic digestion of the LPS of the bacteria by the EƐ34 TSP results in a "naked" *S. newington*, which are much sensitive to antimicrobial agents. This phenomenon might be the cause of the bacteria killing observed by the combination treatment of EƐ34 TSP and V. sup as well as the combination treatment observed in Ɛ34 phage and V. sup. Cell culture supernatants are known to contain antimicrobial peptides **[95],** activated complement proteins **[96]** which mediate killing of bacteria by membrane attack. The

Preprints (www.preprints.org) | NOT PEER-REVIEWED | Posted: 21 October 2021 doi:10.20944/preprints202110.0308.v1

antimicrobial peptides found in cell culture supernatant effect their antibacterial activity through membrane integrity disruption **[97]**. Majority of these peptides are positively charged peptides and they interact with the negative charges found in the LPS of the *S. newington*. Most resistance mechanism against antibacterial peptides such as found in serum or cell culture supernatant include fatty acid additions, acetylation of the O-antigen, and hydroxylation of fatty acids of the LPS. These modifications play significant role in immune evasion, and maintenance of the bacteria virulent phenotypes **[98,99].** Lyses of the bacteria through lytic cycle of the phage will inhibits the bacteria growth (**Figure 1B**). However, this phage can also undergo lysogeny, which interestingly is a maneuver used to block superinfection after lysogenization **[100]**. This is to ensure the survival of its host and hence prolonged incubation in the phage usually can lead to growth of the bacteria **(Figure 1B)**. In the presence of Vero cell culture supernatant however, the results seem to indicate that lysogenized *S. newington* cells even if they could block superinfection, yet they are less resistant to Vero cell culture supernatant killing. This might have been mediated by the antimicrobial peptide present in the V. sup which are encountering "naked" bacteria.

After testing the sensitivity of EƐ34 TSP to trypsin in the absence of denaturing conditions, and in the presence of sodium dodecyl sulfate at physiological temperature, we observed that EƐ34 TSP showed resistance to the protease except a proteolytic cleavage of the fusion peptide. Nonetheless, partial sensitivity of both undigested and rEK digested samples to trypsin was observed when samples were subjected to long exposure to high SDS concentrations (**Figure 3B**). The molecular weights of the large fragments produced after EƐ34 TSP treatment with trypsin was determined to be 65 KDa by heat unfolding of the resulting fragments. The 65 KDa size monomer is the approximate size of the wild-type Ɛ34 TSP monomer or the size of MƐ34 monomer. We infer that these monomers arose from the largest fragment of EƐ34 TSP (the 123 KDa fragment as in lane 4 (**Figure 3B**) after trypsin treatment that migrated at equivalent weight to the rEK digest samples. In contrast, the lower fragment species were either fully proteolysed within quenching and reheating process or are those species that registered a band at the 25KDa size as indicated in **Figure 3B,** lane 5. The data illustrate that EƐ34 TSP is susceptible to trypsin via the 43 amino acid fusion peptide only at physiological temperatures even after prolonged incubation time of 6 h (**Figure 3A**), however in the same condition, when SDS was added as depicted in **Figure 3B,** lane 4, we observed a number of fragments (123, 85, 78 and 70 KDa) in contrast to the single fragment (123 KDa) observed as in SDS free experiments **Figure 3A** lane 4. This indicates that the presence of SDS was able to de-stabilize some of the EƐ34 TSP species to a degree that made them solvent and enzyme accessible and therefore susceptible to trypsin digestion in sites interior to the protein other than only the 43-amino acid fusion peptide. Another important observation worth mentioning is the shift from blurry band as observed in untreated unheated samples to complete discreet single bands of the EƐ34 TSP after tryptic digest (**Figure 3A**), a similar phenomenon is observed when the protein is digested with rEK only. An exhaustive review by Peter R. Weigele and Co. suggested a general sturdy nature of the β-helix domain in all TSPs and other proteins that have this motif in their constitution **[101]**. Published findings concerning the robust nature of the β -barrel motif that they are usually protease, heat and detergent resistant **[102-104]**. As a control, P22 TSP and matured Ɛ34 TSPs were also treated with trypsin. While it was obvious from the band migration that MƐ34 TSP was resistant to trypsin (**Figure 3A**) similar to P22 TSP, the EƐ34 TSP showed sensitivity at the N-terminally fused peptide. The tailspike protein of Ɛ34 phage possesses similar functionality and may likewise have structural stability approximating that of the P22 phage TSP. Although, most structures that mediate viral adhesion and therefore infection do vary, a broad generalization of similarities is shared in their elongated β-sheet topologies. They possess a unique repetitive fold that consists of β-helix domain. Several bacterial and fungal protein motifs that are implicated in human infectious disease such as those of toxins, virulence factors, adhesins, and surface proteins of *Chlamydia, Helicobacteria, Bordetella, Leishmania, Borrelia, Rickettsia, Neisseria,* and *Bacillus anthracis* are known to contain similar parallel β-helix folds **[105-107].** Some tailspike proteins of other viruses similar to that of Ɛ34 and P22 are also shown to demonstrate protease resistance and stability in the presence of detergents at room temperature. These characteristics are indicative of the role of TSPs as exterior virion structures that must withstand harsh environmental conditions **[108]**. Most β-sheet proteins have been well studied; the first to appear in literature was the pectate lysates from the Erwinia species whose motif is utilized for the infection of plant cells **[109,110].** Beta-sheet proteins similar to that in Ɛ34 TSP are known for their solenoid-shaped or elongated coil structure, typically having the β-strands running orthogonally to the long axis. Most of the P22-like phages such as P22, SF6, and E15 have been shown to possess this motif, which functions dually as a host receptor recognition structure and a LPS attachment and cleavage mechanism **[111-113].** To engineer an antibacterial peptide or protein, there is the need to consider the physiological conditions

Preprints (www.preprints.org) | NOT PEER-REVIEWED | Posted: 21 October 2021 doi:10.20944/preprints202110.0308.v1

as well as the gut conditions if the drug has to be taken orally. Among some of the important factors to consider is proteases e.g. trypsin. Our evaluation of EƐ34 TSP performance against trypsin indicates that it is resistant to the protease and can be formulated as an oral agent to control Salmonella colonization of the human gut.

Another major concern is the formation of biofilm on implants **[114]**, transplants scaffold biomaterials **[115]** and on clinical instruments such as catheters etc. **[116-118].** There is an extensive failure of antibiotic treatment to eradicate biofilm-associated infections **[119-122].** This warrants research into biofilm prevention strategies. Currently, majority of biofilm control strategies include prevention of contamination, reducing the ability of bacterial attachment, use of antibiotics or agents that can penetrate and remove biofilm matrix **[123,124].** The use of phages to fight biofilm accumulation has been investigated **[125]**. Cerca et al., 2007 used phage K to reduce Staph. epidermidis biofilm biomass **[126]**, Kelly et al., 2012 reported the inhibition of Staphylococcus aureus biofilm formation using phage K and modified derivatives **[127]**. Using a broad lytic *Salmonella* phage to control biofilm accumulation in food matrices have also been investigated **[128]**. In this work (**Figures 8 and 9**), we investigated the ability of Ɛ34 phage, EƐ34 TSP, or their combination with Vero cell culture supernatant to prevent *S. newington* biofilm formation and accumulation on decellularized avian cartilage construct over 48 h period. While the control showed high accumulation of *S. newington* biofilm in 36 h time point (**Figures 8 and 9)**, the Ɛ34 phage and EƐ34 TSP and their Vero cell culture combination treatment significantly reduced *S. newington* biofilm accumulation on decellularized avian cartilage scaffolds in both 36 h time point (**Figures 8 and 9)**. Additionally, via DAPI and propidium iodide staining analysis of the biofilm formation indicated significantly less biofilm accumulation in the decellularized scaffolds treated to EƐ34 TSP and Vero cell culture supernatant than all other treatment groups (**Figure 8**). The performance of Ɛ34 phage and Vero cell culture supernatant combination showed similar results as the EƐ34 TSP and Vero cell culture supernatant combination, a fascinating result that indicate that Vero cell culture supernatant produces synergetic biofilm inhibition ability to both Ɛ34 phage and EƐ34 TSP. Ɛ34 phage possess the O-antigen hydrolase **[129]** which is the tailspike protein (TSP) which binds to the LPS of *S. newington* initiate infection. Lyses of the bacteria through lytic cycle of the phage will reduce the bacterial survival and hence prevent biofilm accumulation. However, this phage can also undergo lysogeny, which interestingly is a maneuver used to block superinfection after lysogenization **[130]**. This is to ensure the survival of its host. In the presence of Vero cell culture supernatant however, the results seem to indicate that lysogenized *S. newington* cells even if they could block superinfection, yet they are less resistant to Vero cell culture supernatant killing.

The use of SEM to study biofilms has been very instrumental in understanding the morphological details **[131,132]**. In this study (**Figure 10)**, the morphology of the biofilm formed by *S. newington* showed a large and smooth sheath of covering of the decellularized avian cartilage scaffold surface in 36 and 48 h time period for the untreated control samples. In the samples treated with EƐ34 TSP and Vero cell culture combination, we observed an insignificant amount of biofilm accumulation using the SEM. These observations corroborate with our PI staining results.

4 Conclusion

EE34 TSP, a fusion protein engineered using the E34 tailspike gene was demonstrated to possess antibacterial activity against *S. newington* bacterial cells. When combined treatment of the TSP and Vero cell culture supernatant was administered to *S. newington*, the results showed a complete eradication of the bacteria. Also, when decellularized avian scaffold was pretreated with EE34 TSP, or EE34 TSP in Vero cell culture supernatant it inhibited *S. newington's* biofilm formation. Computational analysis of the putative receptor-E34 TSP interaction showed that E34 TSP binds to ompA of the bacterial cell membrane with high probability and affinity.

The engineered trypsin resistant protein therefore can be made into an orally administered antibacterial agent for the control of *Salmonella* in both animals and humans. For this reason we considered the effects the digestive enzyme trypsin (a component of gut environment) on the protein. Our evaluation of EƐ34 TSP performance against trypsin indicates that it is resistant to the protease and can be formulated as an oral agent to control *Salmonella* colonization of the human gut.

Acknowledgements

We thank the department of Microbiology, Faculty of Science, Mathematics and Technology, Alabama State University for support.

Conflict of interest: All authors declare that they have no conflicts of interest.

Ethical Approval: This article does not contain any studies with human participants or animals

Preprints (www.preprints.org) | NOT PEER-REVIEWED | Posted: 21 October 2021 doi:10.20944/preprints202110.0308.v1

References

1. Sundin, G.W. and Wang, N., 2018. Antibiotic resistance in plant-pathogenic bacteria. Annual Review of phytopathology, 56, pp.161-180.
2. Sørum, H. and Sunde, M., 2001. Resistance to antibiotics in the normal flora of animals. Veterinary research, 32(3-4), pp.227-241.
3. Sandoval-Motta, Santiago, and Maximino Aldana. "Adaptive resistance to antibiotics in bacteria: a systems biology perspective." Wiley Interdisciplinary Reviews: Systems Biology and Medicine 8, no. 3 (2016): 253-267.
4. Chattopadhyay MK, Jagannadham MV. Vesicles-mediated resistance to antibiotics in bacteria. Frontiers in microbiology. 2015 Jul 23;6:758.
5. Lopatkin, A. J., & Yang, J. H. (2021). Digital Insights Into Nucleotide Metabolism and Antibiotic Treatment Failure. Frontiers in digital health, 3, 583468. https://doi.org/10.3389/fdgth.2021.583468
6. Graham, D.Y., 1998. Antibiotic resistance in Helicobacter pylori: implications for therapy. Gastroenterology, 115(5), pp.1272-1277.
7. Levy, S.B., 2001. Antibiotic resistance: consequences of inaction. *Clinical Infectious Diseases*, *33*(Supplement_3), pp.S124-S129.
8. Lambert, PA1308633. "Mechanisms of antibiotic resistance in Pseudomonas aeruginosa." Journal of the royal society of medicine 95, no. Suppl 41 (2002): 22.
9. Munita, J.M. and Arias, C.A., 2016. Mechanisms of antibiotic resistance. Microbiology spectrum, 4(2), pp.4-2.
10. Opal, S.M. and Pop-Vicas, A., 2015. 18-Molecular Mechanisms of Antibiotic Resistance in Bacteria. Mandell, Douglas, and Bennett's Principles and Practice of Infectious Diseases, pp.235-251.
11. Maiden MC. Horizontal genetic exchange, evolution, and spread of antibiotic resistance in bacteria. Clin Infect Dis. 1998 Aug;27 Suppl 1:S12-20. doi: 10.1086/514917. PMID: 9710667.
12. Hernando-Amado, S., Coque, T. M., Baquero, F., & Martinez, J. L. (2020). Antibiotic Resistance: Moving From Individual Health Norms to Social Norms in One Health and Global Health. *Front Microbiol*, *11*, 1914. https://doi.org/10.3389/fmicb.2020.01914
13. Schrader SM, Vaubourgeix J, Nathan C. Biology of antimicrobial resistance and approaches to combat it. Sci Transl Med. 2020 Jun 24;12(549): eaaz6992. doi: 10.1126/scitranslmed.aaz6992. PMID: 32581135; PMCID: PMC8177555.
14. Barlow, M. (2009). What antimicrobial resistance has taught us about horizontal gene transfer. *Methods Mol Biol*, *532*, 397-411. https://doi.org/10.1007/978-1-60327-853-9_23
15. Centers for Disease Control and Prevention (CDC). National Salmonella Surveillance Overview. Atlanta, Georgia: US Department of Health and Human Services, CDC, 2011. http://www.cdc.gov/nationalsurveillance/PDFs/NationalSalmSurveillOverview_508.pdf (accessed 10/25/2012
16. Gast, R.K. and Porter Jr, R.E., 2020. Salmonella infections. *Diseases of poultry*, pp.717-753.
17. Maura, D. and Debarbieux, L., 2011. Bacteriophages as twenty-first century antibacterial tools for food and medicine. Applied microbiology and biotechnology, 90(3), pp.851-859.
18. Buttimer, C. ed., 2020. Bacterial Viruses: Exploitation for Biocontrol and Therapeutics. Caister Academic Press.
19. Kropinski, A.M., Sulakvelidze, A., Konczy, P. and Poppe, C., 2007. Salmonella phages and prophages—genomics and practical aspects. Salmonella, pp.133-175.
20. Harada, Kenji, Mitsuo Kameda, Mitsue Suzuki, and Susumu Mitsuhashi. "Mutant of Salmonella phage epsilon 34 with loss of converting ability." Japanese journal of microbiology 8, no. 4 (1964): 125-130.
21. Zayas, M.V. and Villafane, R., 2007. The tailspike protein of the Salmonella phage [epsilon] 34.

Preprints (www.preprints.org) | NOT PEER-REVIEWED | Posted: 21 October 2021 doi:10.20944/preprints202110.0308.v1

22. Harada, K., Kameda, M., Suzuki, M. and Mitsuhashi, S., 1964. DRUG RESISTANCE OF ENTERIC BACTERIA III. FR (TC) Acquisition of Transferability of Nontransmissible R (TC) Factor in Cooperation With F Factor and Formation of. Journal of bacteriology, 88(5), pp.1257-1265.
23. Ayariga, J. A., Venkatesan, K., Ward, R., Wu, H, Jackson, D., Villafane, R. (2018). Initiation of P22 Infection at the Phage Centennial. Front. Sci. Technol. Eng. Math. 2, 64-81.
24. Mansour, S.C., Pena, O.M. and Hancock, R.E., 2014. Host defense peptides: front-line immunomodulators. Trends in immunology, 35(9), pp.443-450.
25. Brightbill, H.D., Libraty, D.H., Krutzik, S.R., Yang, R.B., Belisle, J.T., Bleharski, J.R., Maitland, M., Norgard, M.V., Plevy, S.E., Smale, S.T. and Brennan, P.J., 1999. Host defense mechanisms triggered by microbial lipoproteins through toll-like receptors. Science, 285(5428), pp.732-736.
26. Beckman, J.S. and Crow, J.P., 1993. Pathological implications of nitric oxide, superoxide and peroxynitrite formation. Biochemical Society Transactions, 21(2), pp.330-334.
27. Phoenix, D.A., Dennison, S.R. and Harris, F., 2013. Antimicrobial peptides: their history, evolution, and functional promiscuity. Antimicrobial peptides, 8, pp.1-37.
28. Zasloff, M., 2002. Antimicrobial peptides of multicellular organisms. nature, 415(6870), pp.389-395.
29. Mansour, S.C., Pena, O.M. and Hancock, R.E., 2014. Host defense peptides: front-line immunomodulators. Trends in immunology, 35(9), pp.443-450.
30. Epand, R.F., Mowery, B.P., Lee, S.E., Stahl, S.S., Lehrer, R.I., Gellman, S.H. and Epand, R.M., 2008. Dual mechanism of bacterial lethality for a cationic sequence-random copolymer that mimics host-defense antimicrobial peptides. Journal of molecular biology, 379(1), pp.38-50.
31. Nicolas, P., 2009. Multifunctional host defense peptides: intracellular-targeting antimicrobial peptides. The FEBS journal, 276(22), pp.6483-6496.
32. Hale, J.D. and Hancock, R.E., 2007. Alternative mechanisms of action of cationic antimicrobial peptides on bacteria. Expert review of anti-infective therapy, 5(6), pp.951-959.
33. Fjell, C.D., Hiss, J.A., Hancock, R.E. and Schneider, G., 2012. Designing antimicrobial peptides: form follows function. Nature reviews Drug discovery, 11(1), pp.37-51.
34. Harder, J., Bartels, J., Christophers, E. and Schröder, J.M., 2001. Isolation and Characterization of Human μ-Defensin-3, a Novel Human Inducible Peptide Antibiotic. Journal of Biological Chemistry, 276(8), pp.5707-5713.
35. Roach, D.R. and Donovan, D.M., 2015. Antimicrobial bacteriophage-derived proteins and therapeutic applications. Bacteriophage, 5(3), p.e1062590.
36. Roach D. R., Leung C. Y., Henry M., Morello E., Singh D., Di Santo J. P., et al. (2017). Synergy between the host immune system and bacteriophage is essential for successful phage therapy against an acute respiratory pathogen. Cell Host Microbe 22 38.e–47.e. 10.1016/j.chom.2017.06.018 [PubMed] [CrossRef] [Google Scholar]
37. Ayariga, J.A., Gildea, L., Wu, H. and Villafane, R., 2021. The Ɛ34 Phage Tailspike Protein: An in vitro characterization, Structure Prediction, Potential Interaction with S. newington LPS and Cytotoxicity Assessment to Animal Cell Line. bioRxiv.
38. Garcia E. F., Luciano W. A., Xavier D. E., et al. Identification of lactic acid bacteria in fruit pulp processing byproducts and potential probiotic properties of selected *Lactobacillus* strains. *Frontiers in Microbiology.* 2016;7:p. 1317. doi: 10.3389/fmicb.2016.01371.
39. Qian, Z., Zhao, D., Yin, Y., Zhu, H., & Chen, D. (2020). Antibacterial Activity of Lactobacillus Strains Isolated from Mongolian Yogurt against Gardnerella vaginalis. BioMed research international, 2020, 3548618. https://doi.org/10.1155/2020/3548618

Preprints (www.preprints.org) | NOT PEER-REVIEWED | Posted: 21 October 2021 doi:10.20944/preprints202110.0308.v1

40. Li, L., Finnegan, M.B., Özkan, S., Kim, Y., Lillehoj, P.B., Ho, C.M., Lux, R., Mito, R., Loewy, Z. and Shi, W., 2010. In vitro study of biofilm formation and effectiveness of antimicrobial treatment on various dental material surfaces. Molecular oral microbiology, 25(6), pp.384-390.
41. Li, D., Zhang, L., Liang, J., Deng, W., Wei, Q., & Wang, K. (2021). Biofilm Formation by Pseudomonas aeruginosa in a Novel Septic Arthritis Model. Frontiers in cellular and infection microbiology, 11, 724113. https://doi.org/10.3389/fcimb.2021.724113
42. Arnold K, Bordoli L, Kopp J, Schwede T. 2006. The SWISS-MODEL workspace: a web-based environment for protein structure homology modeling. Bioinformatics, 2: 195–201.
43. Bordoli L, Kiefer F, Arnold K, Benkert P, Battey J, Schwede T. 2009. Protein structure homology modeling using SWISS-MODEL workspace. Nature Protocols, 1: 1–13.
44. Filiz, Ertuğrul, and İ. Koç. "In silico sequence analysis and homology modeling of predicted beta-amylase 7-like protein in Brachypodium distachyon." *LJ BioSci Biotechnol* 3, no. 1 (2014): 61-67.
45. Pautsch, A., & Schulz, G. E. (1998). Structure of the outer membrane protein A transmembrane domain. Nature structural biology, 5(11), 1013–1017. https://doi.org/10.1038/2983
46. Zeng, H., Wang, S., Zhou, T., Zhao, F., Li, X., Wu, Q., & Xu, J. (2018). ComplexContact: a web server for inter-protein contact prediction using deep learning. *Nucleic acids research*, *46*(W1), W432–W437. https://doi.org/10.1093/nar/gky420
47. Tianming Zhou, Sheng Wang and Jinbo Xu. Deep learnign reveals many more inter-protein contacts than direct coupling analysis. RECOMB 2018.
48. Sheng Wang, Siqi Sun and Jinbo Xu. Analysis of deep learning methods for blind protein contact prediction in CASP12. PROTEINS, 2017
49. Sheng Wang, Siqi Sun, Zhen Li, Renyu Zhang and Jinbo Xu. Accurate De Novo Prediction of Protein Contact Map by Ultra-Deep Learning Model. PLoS Computational Biology, 2017.
50. Zeng, H., Wang, S., Zhou, T., Zhao, F., Li, X., Wu, Q., & Xu, J. (2018). ComplexContact: a web server for inter-protein contact prediction using deep learning. Nucleic acids research, 46(W1), W432–W437. https://doi.org/10.1093/nar/gky420
51. Pier Paolo Olimpieri, Anna Chailyan, Anna Tramontano, Paolo Marcatili, Prediction of site-specific interactions in antibody-antigen complexes: the proABC method and server, *Bioinformatics*, Volume 29, Issue 18, 15 September 2013, Pages 2285–2291, https://doi.org/10.1093/bioinformatics/btt369.
52. Movva NR, Nakamura K, Inouye M. Amino acid sequence of the signal peptide of ompA protein, a major outer membrane protein of Escherichia coli. J Biol Chem. 1980 Jan 10;255(1):27-9. PMID: 6985608.
53. Spike protein recognizer receptor ACE2 targeted identification of potential natural antiviral drug candidates against SARS-CoV-2 Pokhrel S, Bouback TA, Samad A, Nur SM, Alam R, Abdullah-Al-Mamun M, Nain Z, Imon RR, Talukder MEK, Tareq MMI, Hossen MS, Karpiński TM, Ahammad F, Qadri I, Rahman MS. Int J Biol Macromol. 2021 Sep 27;S0141-8130(21)02075-4.
54. Dallakyan S., Olson A.J. Chemical Biology. Humana Press; New York, NY: 2015. Small-molecule library screening by docking with PyRx; pp. 243–250.
55. Ayariga, J.A., Gildea, L., Wu, H. and Villafane, R., 2021. The Ɛ34 Phage Tailspike Protein: An in vitro characterization, Structure Prediction, Potential Interaction with S. newington LPS and Cytotoxicity Assessment to Animal Cell Line. bioRxiv.

Preprints (www.preprints.org) | NOT PEER-REVIEWED | Posted: 21 October 2021 doi:10.20944/preprints202110.0308.v1

56. Greenfield J, Shang X, Luo H. Zhou Y, Heselpoth RD, Nelson DC, Herzberg O. 2019. Structure and tailspike glycosidase machinery of ORF212 from E. coli O157:H7 phage CBA120 (TSP3). Sci Rep 9, 7349 https://doi.org/10.1038/s41598-019-43748-9
57. X. Carbonell, A. Villaverde. 1998. Unfolding of bacteriophage P22 TSP: Enhanced thermal stability of an N-Terminal fusion mutant, FEBS letters. Vol. 432, Issue. 3. Pages 228-230
58. X. Carbonell, A. Villaverde. 1998. Unfolding of bacteriophage P22 TSP: Enhanced thermal stability of an N-Terminal fusion mutant, FEBS letters. Vol. 432, Issue. 3. Pages 228-230
59. Freiberg, A., Morona, R., Van Den Bosch, L., Jung, C., Behlke, J., Carlin, N., Seckler, R. and Baxa, U., 2003. The tailspike protein of Shigella phage Sf6: A structural homolog of Salmonella phage P22 tailspike protein without sequence similarity in the β-helix domain. Journal of Biological Chemistry, 278(3), pp.1542-1548.
60. Ayariga, J.A., Gildea, L., Wu, H. and Villafane, R., 2021. The Ɛ34 Phage Tailspike Protein: An in vitro characterization, Structure Prediction, Potential Interaction with S. newington LPS and Cytotoxicity Assessment to Animal Cell Line. bioRxiv.
61. Fuchs, A., Seiderer, C. and Seckler, R., 1991. In vitro folding pathway of phage P22 tailspike protein. Biochemistry, 30(26), pp.6598-6604.
62. Spatara, M.L., Roberts, C.J. and Robinson, A.S., 2009. Kinetic folding studies of the P22 tailspike beta-helix domain reveal multiple unfolded states. Biophysical chemistry, 141(2-3), pp.214-221.
63. Schuler, B., Fürst, F., Osterroth, F., Steinbacher, S., Huber, R. and Seckler, R., 2000. Plasticity and steric strain in a parallel β-helix: Rational mutations in the P22 tailspike protein. Proteins: Structure, Function, and Bioinformatics, 39(1), pp.89-101.
64. Hathroubi, S., Servetas, S.L., Windham, I., Merrell, D.S. and Ottemann, K.M., 2018. Helicobacter pylori biofilm formation and its potential role in pathogenesis. Microbiology and Molecular Biology Reviews, 82(2), pp.e00001-18.
65. Donlan, R.M., 2001. Biofilm formation: a clinically relevant microbiological process. Clinical infectious diseases, 33(8), pp.1387-1392.
66. Ghosh, A., Jayaraman, N. and Chatterji, D., 2020. Small-molecule inhibition of bacterial biofilm. ACS omega, 5(7), pp.3108-3115.
67. Reen, F.J., Gutiérrez-Barranquero, J.A. and Parages, M.L., 2018. Coumarin: a novel player in microbial quorum sensing and biofilm formation inhibition. Applied Microbiology and Biotechnology, 102(5), pp.2063-2073.
68. Rajkumari, J., Borkotoky, S., Reddy, D., Mohanty, S.K., Kumavath, R., Murali, A., Suchiang, K. and Busi, S., 2019. Anti-quorum sensing and anti-biofilm activity of 5-hydroxymethylfurfural against Pseudomonas aeruginosa PAO1: Insights from in vitro, in vivo and in silico studies. Microbiological research, 226, pp.19-26.
69. Yu, M. and Chua, S.L., 2020. Demolishing the great wall of biofilms in Gram-negative bacteria: To disrupt or disperse? Medicinal research reviews, 40(3), pp.1103-1116.
70. Pires, D.P., Melo, L.D., Boas, D.V., Sillankorva, S. and Azeredo, J., 2017. Phage therapy as an alternative or complementary strategy to prevent and control biofilm-related infections. Current opinion in microbiology, 39, pp.48-56.
71. Pires, D.P., Melo, L.D., and Azeredo, J., 2021. Understanding the Complex Phage-Host Interactions in Biofilm Communities. Annual Review of Virology, 8(1), 73-94.
72. Tkhilaishvili, T., Lombardi, L., Klatt, A.B., Trampuz, A. and Di Luca, M., 2018. Bacteriophage Sb-1 enhances antibiotic activity against biofilm, degrades exopolysaccharide matrix and targets persisters of Staphylococcus aureus. International Journal of Antimicrobial Agents, 52(6), pp.842-853.
73. Harper, D.R., Parracho, H.M., Walker, J., Sharp, R., Hughes, G., Werthén, M., Lehman, S. and Morales, S., 2014. Bacteriophages and biofilms. Antibiotics, 3(3), pp.270-284.

Preprints (www.preprints.org) | NOT PEER-REVIEWED | Posted: 21 October 2021 doi:10.20944/preprints202110.0308.v1

74. Tkhilaishvili, Tamta, Lisa Lombardi, Ann-Brit Klatt, Andrej Trampuz, and Mariagrazia Di Luca. "Bacteriophage Sb-1 enhances antibiotic activity against biofilm, degrades exopolysaccharide matrix and targets persisters of Staphylococcus aureus." International Journal of Antimicrobial Agents 52, no. 6 (2018): 842-853.
75. Taylor, P.W., 1983. Bactericidal and bacteriolytic activity of serum against gram-negative bacteria. Microbiological reviews, 47(1), pp.46-83.
76. Clas, F., Schmidt, G. and Loos, M., 1985. The role of the classical pathway for the bactericidal effect of normal sera against gram-negative bacteria. Bacteria and Complement, pp.19-72.
77. Rowley, D., 1968. Sensitivity of rough gram-negative bacteria to the bactericidal action of serum. Journal of bacteriology, 95(5), pp.1647-1650.
78. Marr, A.K., Gooderham, W.J. and Hancock, R.E., 2006. Antibacterial peptides for therapeutic use: obstacles and realistic outlook. *Current opinion in pharmacology*, *6*(5), pp.468-472.
79. Montenegro, M.A., Bitter-Suermann, D., Timmis, J.K., Agüero, M.E., Cabello, F.C., Sanyal, S.C. and Timmis, K.N., 1985. traT gene sequences, serum resistance and pathogenicity-related factors in clinical isolates of Escherichia coli and other gram-negative bacteria. Microbiology, 131(6), pp.1511-1521.
80. Zeng, H., Wang, S., Zhou, T., Zhao, F., Li, X., Wu, Q., & Xu, J. (2018). ComplexContact: a web server for inter-protein contact prediction using deep learning. Nucleic acids research, 46(W1), W432–W437. https://doi.org/10.1093/nar/gky420
81. "Salmonella Genotype and Phenotype Association." Chen Y., Folster J., Ayers S., Kabera C., Li C., Mukherjee S., Lam C., Zhao S., McDermott P. Submitted (SEP-2014) to the EMBL/GenBank/DDBJ databases Cited for: NUCLEOTIDE SEQUENCE [LARGE SCALE GENOMIC DNA]. Category: Sequences. Strain: CVM N32045Imported.Source: UniProtKB/TrEMBL (unreviewed).
82. 2**"Complete Genome Sequencing of a Multidrug-Resistant and Human-Invasive Salmonella enterica Serovar Typhimurium Strain of the Emerging Sequence Type 213 Genotype."** Calva E., Silva C., Zaidi M.B., Sanchez-Flores A., Estrada K., Silva G.G., Soto-Jimenez L.M., Wiesner M., Fernandez-Mora M., Edwards R.A., Vinuesa P. Genome Announc. 3:e00663-15(2015) [PubMed] [Europe PMC] [Abstract]. *Cited for:* NUCLEOTIDE SEQUENCE [LARGE SCALE GENOMIC DNA]. *Category:* Sequences. *Strain:* YU39Imported. *Source:* UniProtKB/TrEMBL (unreviewed). *This publication is cited by 4896 other entries.*
83. **"Characterization of the Virulence Potential of Salmonella enterica Isolates Carrying Incompatibility Group FIB Plasmids using Caco-2 Intestinal Epithelial Cells."** Sanad Y., Khajanchi B., Deck J., Cox J., Thaker R., Han J., Nayak R., Foley S. Submitted (NOV-2017) to the EMBL/GenBank/DDBJ databases. *Cited for:* NUCLEOTIDE SEQUENCE [LARGE SCALE GENOMIC DNA]. *Category:* Sequences. *Strain:* N029Imported. *Source:* UniProtKB/TrEMBL (unreviewed)
84. **"SKESA: strategic k-mer extension for scrupulous assemblies."** Souvorov A., Agarwala R., Lipman D.J. Genome Biol. 19:153-150(2018) [PubMed] [Europe PMC] [Abstract]. *Cited for:* NUCLEOTIDE SEQUENCE. *Category:* Sequences.
85. "Salmonella typhimurium outer membrane protein A (ompA) gene." Nouri M., Rahbarizadeh F., Moosakhani F., Farokhimanesh S., Aghaei Bakhtiari S.H. Submitted (APR-2007) to the EMBL/GenBank/DDBJ databases. Cited for: NUCLEOTIDE SEQUENCE. Category: Sequences. Source: UniProtKB/TrEMBL (unreviewed).
86. Kataria J.L., Kumar A., Sailo B., Lalsiamthara J., Lalrinkima H., Kamble N.M., Kumar P., Agarwal R.K. Submitted (FEB-2013) to the EMBL/GenBank/DDBJ databases. Cited for: NUCLEOTIDE SEQUENCE. Category: Sequences. Strain: E-2375Imported. Source: UniProtKB/TrEMBL (unreviewed).

Preprints (www.preprints.org) | NOT PEER-REVIEWED | Posted: 21 October 2021 doi:10.20944/preprints202110.0308.v1

87. "Salmonella distinguishable signature define host species." Yue M., Schifferli D. Submitted (JAN-2014) to the EMBL/GenBank/DDBJ databases. Cited for: NUCLEOTIDE SEQUENCE. Category: Sequences. Strain: OmpA1
88. "Salmonella distinguishable signature define host species." Yue M., Schifferli D. Submitted (JAN-2014) to the EMBL/GenBank/DDBJ databases. Cited for: NUCLEOTIDE SEQUENCE. Category: Sequences. Strain: OmpN1
89. "Salmonella Genotype and Phenotype Association." Chen Y., Folster J., Ayers S., Kabera C., Li C., Mukherjee S., Lam C., Zhao S., McDermott P. Submitted (SEP-2014) to the EMBL/GenBank/DDBJ databases. Cited for: NUCLEOTIDE SEQUENCE [LARGE SCALE GENOMIC DNA]. Category: Sequences. Strain: CVM N32045Imported.Source: UniProtKB/TrEMBL (unreviewed).
90. Complete Genome Sequencing of a Multidrug-Resistant and Human-Invasive Salmonella enterica Serovar Typhimurium Strain of the Emerging Sequence Type 213 Genotype." Calva E., Silva C., Zaidi M.B., Sanchez-Flores A., Estrada K., Silva G.G., Soto-Jimenez L.M., Wiesner M., Fernandez-Mora M., Edwards R.A., Vinuesa P. Genome Announc. 3:e00663-15(2015) [PubMed] [Europe PMC] [Abstract]. Cited for: NUCLEOTIDE SEQUENCE [LARGE SCALE GENOMIC DNA]. Category: Sequences. Strain: YU39Imported
91. Characterization of the Virulence Potential of Salmonella enterica Isolates Carrying Incompatibility Group FIB Plasmids using Caco-2 Intestinal Epithelial Cells." Sanad Y., Khajanchi B., Deck J., Cox J., Thaker R., Han J., Nayak R., Foley S. Submitted (NOV-2017) to the EMBL/GenBank/DDBJ databases. Cited for: NUCLEOTIDE SEQUENCE [LARGE SCALE GENOMIC DNA]. Category: Sequences. Strain: N029Imported. Source: UniProtKB/TrEMBL (unreviewed).
92. Characterization of the Virulence Potential of Salmonella enterica Isolates Carrying Incompatibility Group FIB Plasmids using Caco-2 Intestinal Epithelial Cells." Sanad Y., Khajanchi B., Deck J., Cox J., Thaker R., Han J., Nayak R., Foley S. Submitted (NOV-2017) to the EMBL/GenBank/DDBJ databases. Cited for: NUCLEOTIDE SEQUENCE [LARGE SCALE GENOMIC DNA]. Category: Sequences. Strain: N029Imported. Source: UniProtKB/TrEMBL (unreviewed).
93. “Salmonella distinguishable signature define host species." Yue M., Schifferli D. Submitted (JAN-2014) to the EMBL/GenBank/DDBJ databases. Cited for: NUCLEOTIDE SEQUENCE. Category: Sequences. Strain: OmpC10
94. "Cloning and characterization of ompC of Salmonella enterica serovar Typhimurium (E-2375)." Prejit N., Agarwal R.K., Bhilegaonkar K., Biswas R., Bagath M., Kumar K. Submitted (JUN-2009) to the EMBL/GenBank/DDBJ databases. Cited for: NUCLEOTIDE SEQUENCE. Category: Sequences. Strain: E-2375Imported. Source: UniProtKB/TrEMBL (unreviewed).
95. Hancock, R.E. and Scott, M.G., 2000. The role of antimicrobial peptides in animal defenses. Proceedings of the national Academy of Sciences, 97(16), pp.8856-8861.
96. Thomas, A., Gasque, P., Vaudry, D., Gonzalez, B. and Fontaine, M., 2000. Expression of a complete and functional complement system by human neuronal cells in vitro. International immunology, 12(7), pp.1015-1023.
97. Gunn, J.S., 2001. Bacterial modification of LPS and resistance to antimicrobial peptides. Journal of endotoxin research, 7(1), pp.57-62.
98. Gunn, J.S., 2001. Bacterial modification of LPS and resistance to antimicrobial peptides. Journal of endotoxin research, 7(1), pp.57-62.
99. Joo, H.S., Fu, C.I. and Otto, M., 2016. Bacterial strategies of resistance to antimicrobial peptides. Philosophical Transactions of the Royal Society B: Biological Sciences, 371(1695), p.20150292.
100. Kanegasaki, S., & Tomita, T. (1976). Mutants of Salmonella newington that block bacteriophage epsilon infection at early stages. Journal of bacteriology, 127(1), 7–13. https://doi.org/10.1128/jb.127.1.7-13.1976
101. Peter R Weigele, Eben Scanlon, Jonathan King. 2003. Homotrimeric, β-stranded viral adhesins and Tail proteins. Jbac. PP. 4022-4030

Preprints (www.preprints.org) | NOT PEER-REVIEWED | Posted: 21 October 2021 doi:10.20944/preprints202110.0308.v1

102. Steinbacher S, R Seckler, S Miller, B Steipe, R Huber, P Reinemer. 1994. Crystal structure of P22 tailspike protein: interdigitated subunits in a thermostable trimer. Science 265:383-386
103. Milka Zayas, Robert Villafane. 2007. Identification of the Salmonella phage ε34 tailspike gene. Gene: Vol. 386. Issue 1-2. Pages 211 – 217
104. Galaleldeen, A., Taylor, A.B., Chen, D., Schuermann, J.P., Holloway, S.P., Hou, S., Gong, S., Zhong, G. and Hart, P.J., 2013. Structure of the Chlamydia trachomatis immunodominant antigen Pgp3. Journal of Biological Chemistry, 288(30), pp.22068-22079.
105. Tosi, T., Cioci, G., Jouravleva, K., Dian, C. and Terradot, L., 2009. Structures of the tumor necrosis factor α inducing protein Tipα: a novel virulence factor from Helicobacter pylori. FEBS letters, 583(10), pp.1581-1585.
106. Bradley P, L Cowen, M Menke, J King, B Berger. 2001. BETAWRAP: Successful prediction of parallel beta-helices from primary sequence reveals an association with many microbial pathogens. Proc. Natl. Acad. Sci. USA. 98:148119-148224
107. Peter R Weigele, Eben Scanlon, Jonathan King. 2003. Homotrimeric, beta-stranded viral adhesions and Tail proteins. Journal of Bacteriology. 185.14. 4022-4030
108. Jenkins J, R Pickersgill. 2001. The architecture of parallel beta-helices and related folds. Prog. Biophys. Mol. Biol.77:111-175
109. Yoder MD, NT Keen, F Jurnak. 1993. New domain motif; the structure of pectate lysase C, a secreted plant virulence factor. Science 260: 1503-1507
110. Steinbacher S, S Miller, U Baxa, N Budisa, A Weintraub, R Seckler, R Huber. 1996. Crystal structure of phage P22 tailspike protein complexed with Salmonella Sp. O-antigen receptors. Proc. Natl. Acad. Sci. USA: 93: 10584-10588
111. Jeremie Williams, Karthikeya Venkatesan, Joseph Atia Ayariga, Doba Jackson, Hongzhuan Wu, Robert Villafane. 2018. A genetic analysis of an important hydrophobic interaction at the P22 tailspike protein N-terminal domain. Archives of Virology.
112. Ayariga Joseph, Venkatesan Karthikeya, Ward Robert, Wu Hongzhuan, Jackson Doba, Villafan Robert. 2018. Initiation of P22 Infection at the Phage Centennial. Frontiers in Science, Technology, Engineering and Mathematics: A Peer-Reviewed Journal. Vol.2.issue 2.
113. Gominet, M., Compain, F., Beloin, C. and Lebeaux, D., 2017. Central venous catheters and biofilms: where do we stand in 2017. Apmis, 125(4), pp.365-375.
114. Veerachamy, S., Yarlagadda, T., Manivasagam, G. and Yarlagadda, P.K., 2014. Bacterial adherence and biofilm formation on medical implants: a review. Proceedings of the Institution of Mechanical Engineers, Part H: Journal of Engineering in Medicine, 228(10), pp.1083-1099.
115. Kathju, S., Nistico, L., Lasko, L.A. and Stoodley, P., 2010. Bacterial biofilm on monofilament suture and porcine xenograft after inguinal herniorrhaphy. FEMS Immunology & Medical Microbiology, 59(3), pp.405-409.
116. Gominet, M., Compain, F., Beloin, C. and Lebeaux, D., 2017. Central venous catheters and biofilms: where do we stand in 2017?. Apmis, 125(4), pp.365-375.
117. Qu, Y., McGiffin, D., Kure, C., Ozcelik, B., Fraser, J., Thissen, H. and Peleg, A.Y., 2020. Biofilm formation and migration on ventricular assist device drivelines. The Journal of thoracic and cardiovascular surgery, 159(2), pp.491-502.
118. Souza, L.B., Silva-Rocha, W.P., Ferreira, M.R., Soares, L.A.L., Svidzinski, T.I., Milan, E.P., Pires, R.H., Fusco Almeida, A.M., Mendes-Giannini, M.J.S. and Maranhão Chaves, G., 2018. Influence of Eugenia uniflora extract on adhesion to human buccal epithelial cells, biofilm formation, and cell surface hydrophobicity of Candida spp. from the oral cavity of kidney transplant recipients. Molecules, 23(10), p.2418.

Preprints (www.preprints.org) | NOT PEER-REVIEWED | Posted: 21 October 2021 doi:10.20944/preprints202110.0308.v1

119. Ramasamy, M. and Lee, J., 2016. Recent nanotechnology approaches for prevention and treatment of biofilm-associated infections on medical devices. BioMed Research International, 2016.
120. Lazăr, V. and Chifiriuc, M.C., 2010. Medical significance and new therapeutical strategies for biofilm associated infections. Roum Arch Microbiol Immunol, 69(3), pp.125-138.
121. Lynch, A.S. and Abbanat, D., 2010. New antibiotic agents and approaches to treat biofilm-associated infections. Expert opinion on therapeutic patents, 20(10), pp.1373-1387.
122. Sun, F., Qu, F., Ling, Y., Mao, P., Xia, P., Chen, H. and Zhou, D., 2013. Biofilm-associated infections: antibiotic resistance and novel therapeutic strategies. Future Microbiology, 8(7), pp.877-886.
123. Donlan, R.M. and Costerton, J.W., 2002. Biofilms: survival mechanisms of clinically relevant microorganisms. Clinical microbiology reviews, 15(2), pp.167-193.
124. Sun, F., Qu, F., Ling, Y., Mao, P., Xia, P., Chen, H. and Zhou, D., 2013. Biofilm-associated infections: antibiotic resistance and novel therapeutic strategies. Future Microbiology, 8(7), pp.877-886.
125. Azeredo, J. and Sutherland, I.W., 2008. The use of phages for the removal of infectious biofilms. Current pharmaceutical biotechnology, 9(4), pp.261-266.
126. Cerca, N., Oliveira, R. and Azeredo, J. (2007) Susceptibility of Staphylococcus epidermidis planktonic cells and biofilms to the lytic action of Staphylococcus bacteriophage K. Lett Appl Microbiol 45, 313– 317
127. Kelly, D., McAuliffe, O., Ross, R.P. and Coffey, A., 2012. Prevention of Staphylococcus aureus biofilm formation and reduction in established biofilm density using a combination of phage K and modified derivatives. Letters in applied microbiology, 54(4), pp.286-291.
128. Islam, M., Zhou, Y., Liang, L., Nime, I., Liu, K., Yan, T., Wang, X. and Li, J., 2019. Application of a phage cocktail for control of Salmonella in foods and reducing biofilms. Viruses, 11(9), p.841.
129. Iwashita, S. and Kanegasaki, S., 1975. Release of O antigen polysaccharide from Salmonella newington by phage ϵ34. Virology, 68(1), pp.27-34.
130. Kanegasaki, S., & Tomita, T. (1976). Mutants of Salmonella newington that block bacteriophage epsilon infection at early stages. Journal of bacteriology, 127(1), 7–13. https://doi.org/10.1128/jb.127.1.7-13.1976
131. Wi Y. M., Patel R. (2018). Understanding Biofilms and Novel Approaches to the Diagnosis, Prevention, and Treatment of Medical Device-Associated Infections. Infect. Dis. Clin. North Am. 32 (4), 915–929. doi: 10.1016/j.idc.2018.06.009
132. Li, D., Zhang, L., Liang, J., Deng, W., Wei, Q., & Wang, K. (2021). Biofilm Formation by Pseudomonas aeruginosa in a Novel Septic Arthritis Model. Frontiers in cellular and infection microbiology, 11, 724113. https://doi.org/10.3389/fcimb.2021.724113

Preprints (www.preprints.org) | NOT PEER-REVIEWED | Posted: 21 October 2021 doi:10.20944/preprints202110.0308.v1

Supplementary data

Figure 1. Structure quality assessment and validation of ompA model.

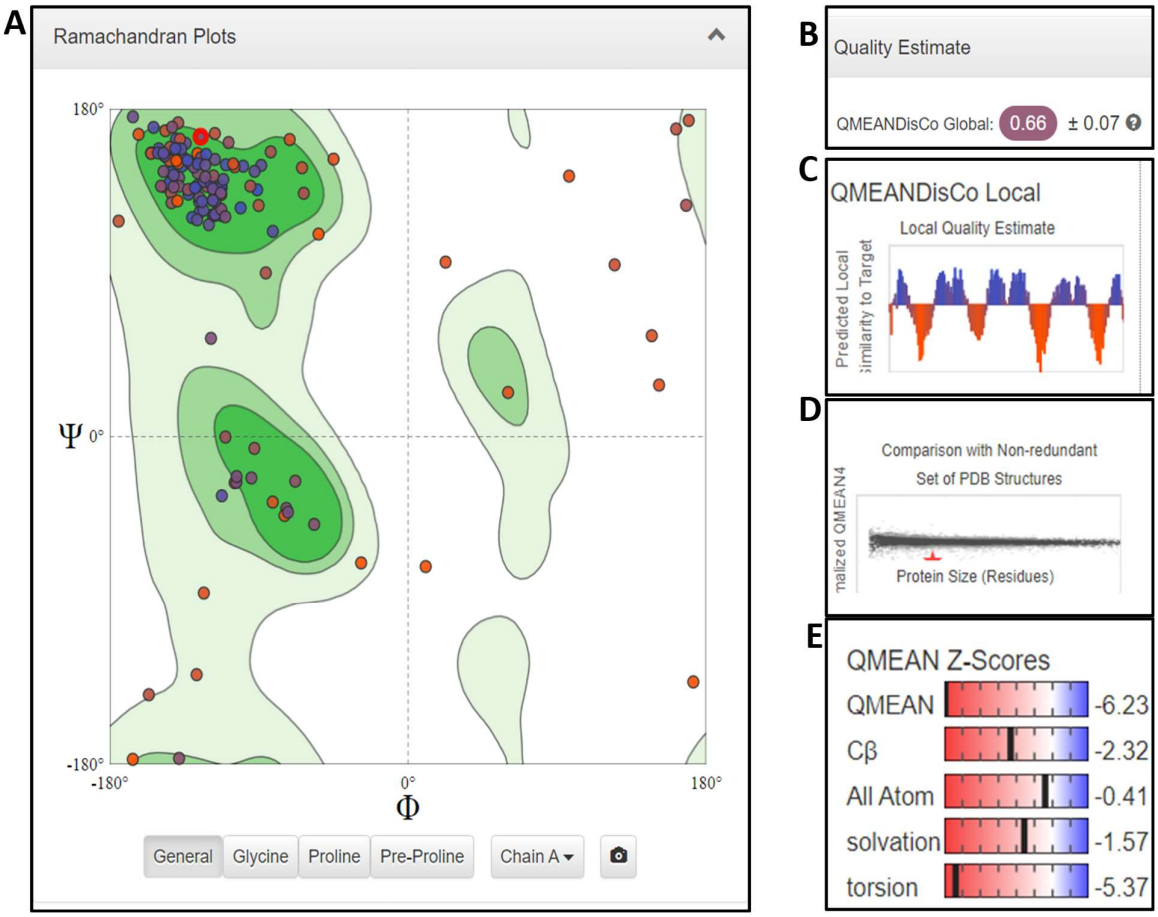

(A) Ramachandran plot analysis of homologue model of ompA of *S. newington*. The analysis showed a molprobity of 2.43 a clash score of 2.32, 86.63% Ramachandran favored structure, 6.98% Ramachandran outliers, 11.11% rotamer outliers and 1 bad bond out of 1377 bonds.

(B) Global quality estimate (QMEANDisCO Global) of 0.66 ±0.07.

(C) Local quality estimate (QMEANDisco Local) depicting residues similarity of the ompA model to target structure.

(D) Comparison of model with non-redundant set of PDB structures, showing that the ompA model score was high as indicated by the red mark.

(E) The QMEAN Z-score of ompA that estimate the absolute quality of the ompA model with reference to solved X-ray crystallographic structures on PDB.